Measuring Entanglement Entropy in Valence Bond Quantum Monte Carlo Simulations

by

Ann Berlinsky Kallin

A thesis
presented to the University of Waterloo
in fulfillment of the
thesis requirement for the degree of
Master of Science
in
Physics

Waterloo, Ontario, Canada, 2010

I hereby declare that I am the sole author of this thesis. This is a true copy of the thesis, including any required final revisions, as accepted by my examiners.

I understand that my thesis may be made electronically available to the public.

Abstract

In this thesis we examine methods for measuring entanglement entropy in spin-1/2 Heisenberg systems using quantum Monte Carlo in the valence bond basis. We begin by presenting the quantum Monte Carlo techniques used in this research. We then use these techniques to directly compare the recently proposed valence bond entanglement entropy to the standard definition of entanglement entropy: the von Neumann entanglement entropy. We find that the valence bond entanglement entropy does not give a bound on the von Neumann entanglement entropy, and that it exhibits a multiplicative logarithmic correction to the area law that is not present in the scaling of the von Neumann entanglement entropy. We then present a method to measure higher orders of the generalized Renyi entanglement entropies using valence bond quantum Monte Carlo, and show results for the second Renyi entropy. We find the results converge to the exact results for one dimensional Heisenberg spin-1/2 chains, and see that the scaling of the second Renyi entropy follows an area law in the two dimensional Heisenberg ground state.

Acknowledgements

I would like to thank my collaborators in this research, Matthew Hastings for his seemingly endless supply of ideas, and Ivan Gonzalez for his expert use of DMRG, also Anders Sandvik for many helpful discussions as well as the creation of most of the techniques used for this research. For many helpful conversations, either scientific or motivational in nature, I would like to thank Jeremy McMinis and both my parents, John Berlinsky and Catherine Kallin. And finally, I would like to acknowledge the incredible patience and enthusiasm of my supervisor, Roger Melko.

Table of Contents

List of Figures

Chapter 1

Introduction

This thesis is an exploration of methods used for the measurement of entanglement in large-scale simulations suitable for condensed matter theory.

In this chapter we discuss different measures of entanglement and their scaling. In Chapter 2 we describe quantum Monte Carlo algorithms in the valence bond basis. Chapter 3 contains measurements of valence bond entanglement entropy compared to the standard von Neumann entanglement entropy. In Chapter 4 we develop a method of measuring all Renyi entanglement entropies, excluding the von Neuman entanglement entropy, using valence bond quantum Monte Carlo. In the final chapter we summarize the results of this research and provide a discussion.

1.1 Quantum Entanglement

Entanglement is one important and interesting feature that differentiates quantum mechanical systems from classical systems. In a pair of entangled spins/particles/photons/states the members of the system have information about each other, even if they are spatially separated. Two spin-1/2 spins, for instance, are considered entangled if their joint state can not be written as the product of their individual states. Of the following two states,

$$|\Psi_{1,2}\rangle = \frac{1}{\sqrt{2}}\big(|\uparrow_1\uparrow_2\rangle + |\downarrow_1\downarrow_2\rangle\big) \qquad \text{and} \qquad |\Phi_{1,2}\rangle = \frac{1}{\sqrt{2}}\big(|\uparrow_1\downarrow_2\rangle - |\downarrow_1\downarrow_2\rangle\big), \tag{1.1}$$

only $|\Phi_{1,2}\rangle$ is separable, and can be rewritten as

$$|\Phi_{1,2}\rangle = \frac{1}{\sqrt{2}}\big(|\uparrow_1\rangle - |\downarrow_1\rangle\big) \otimes |\downarrow_2\rangle. \tag{1.2}$$

Therefore $|\Phi_{1,2}\rangle$ is unentangled, while $|\Psi_{1,2}\rangle$, which cannot be written as a product state, is an entangled state. In the case of two spins it is easy to determine if states are separable (unentangled). As we add more spins to the system it becomes less apparent which states are entangled. Furthermore, we can quantify the degree to which they are entangled beyond being either separable states, or non-separable states (entangled).

1.2 Measures of Entanglement

There are many different quantities that can be used to measure entanglement . Though not exhaustive a few measures include concurrence [1], logarithmic negativity [2], squashed entanglement [3], and entropy of entanglement [4]. Measures of entanglement share three properties [5]:

1. An entanglement measure $E(\rho)$, measuring the entanglement between two spins, is a mapping from density matrices ρ to positive real numbers defined for states of arbitrary bipartite systems. Usually a normalization factor is included such that the maximally entangled state,

$$|\psi_{\max}\rangle = \frac{|\uparrow\uparrow\rangle + |\downarrow\downarrow\rangle}{\sqrt{2}}, \tag{1.3}$$

   of two spins has $E(|\psi_{\max}\rangle\langle\psi_{\max}|) = \ln(2)$.

2. $E(\rho) = 0$ if the state ρ is separable.

3. $E(\rho)$ does not increase under local operators on either of the spins. That is, if we have an operator acting on only *one* of the spins, the entanglement between the two spins will not increase.

There is also a fourth condition, not satisfied by all measures of entanglement, requiring the measure to reduce to the von Neumann entanglement entropy for a system in a pure state.

1.3 The von Neumann Entanglement Entropy

For a system partitioned into two regions, A and B, the von Neumann entanglement entropy S^{vN} is defined as

$$S_{\mathrm{A}}^{\mathrm{vN}} = -\mathrm{Tr}\left(\rho_{\mathrm{A}} \ln \rho_{\mathrm{A}}\right), \tag{1.4}$$

where $\rho_A = \mathrm{Tr}_B|\psi\rangle\langle\psi|$ is the reduced density matrix, the density matrix of the entire system with the degrees of freedom from region B traced out. S^{vN} is only suited to measure the entanglement of a pure state, as is the case for all entanglement measures we will discuss in this thesis. This is due to the way S^{vN} measures entanglement; we begin with a pure state and trace out the degrees of freedom for some subregion B. We are left with ρ_A representing a (possibly mixed) state. S^{vN} can be rewritten in terms of the eigenvalues of the density matrix,

$$S_A^{vN} = -\sum_i (\lambda_i \ln \lambda_i), \tag{1.5}$$

which is quite similar to the form of thermodynamic entropy or Shannon information entropy. If ρ_A represents a pure state, then we *know* what state of region A is in, and ρ_A will have one non-zero eigenvalue equal to 1 (so $S^{vN} = 0$). If ρ_A represents a mixed state, we will have some probability distribution of the possible states (so $S^{vN} > 0$). The entropy of that distribution is used to quantify the entanglement between regions A and B. In the maximally entangled case all eigenvalues are equal to $1/d$ (representing an equal probability of encountering each spin state), where d is the dimension of the Hilbert space for region A (2^N for a system of N spin-1/2 particles). Thus the maximum entanglement entropy for a spin-1/2 system is $S^{vN} = \ln(d) = N\ln(2)$. If the initial state starts off mixed instead of pure, the state would already have some entropy. The entanglement entropy would contain both the initially present classical uncertainty in the state as well as that due to tracing out region B.

The von Neumann entanglement entropy is part of a larger class of entanglement entropies called the generalized Renyi entanglement entropies. The n^{th} Renyi entanglement entropy S_n is defined as

$$S_n(\rho_A) = \frac{1}{1-n} \ln\left[\mathrm{Tr}\left(\rho_A^n\right)\right]. \tag{1.6}$$

Taking the limit $n \to 1$ gives us $S_1 = S^{vN}$. These entanglement entropies have the property that for $n > m$, $S_n \leq S_m$; successive Renyi entropies give a lower bound on the previous entropies [6]. They are useful measures which fully characterize the entanglement entropy of the system.

1.4 Scaling of Entanglement Entropy in Condensed Matter Systems

Using measures of entanglement from quantum information to study interacting quantum many-body systems is a rapidly growing interdisciplinary topic [7, 8]. Entanglement has the advantage of measuring "hidden" correlations which can occur in states where correlation

lengths diverge or decay exponentially. Additionally, measurement of entanglement is independent of the basis chosen to represent the system.

1.4.1 Area Law Scaling

In condensed matter systems, away from special critical points, entanglement entropy typically follows an "area law" [9, 10], perhaps more aptly named a "boundary law", where the entanglement scales with the size of the boundary between two regions (A and B) of the system. In non-critical one-dimensional (1D) systems, for example, the entanglement entropy scales as a constant, since the boundary between regions is zero-dimensional. For two-dimensional (2D) systems we expect the entanglement to scale with the length of the boundary, and in three dimensions the entanglement should scale with the area of the boundary. If S^{vN} has area law scaling for a given system, all Renyi entanglement entropies will follow the same scaling [11]. This area law corresponds to systems with mainly short range entanglement, in which only sites "near" the boundary contribute to the entanglement between regions. If we had a system with extremely long-range entanglement it would be expected that the entire region A is entangled with region B, and one could see a "volume law" scaling of entanglement. However, this area law is expected to hold for the ground states of many interacting quantum systems.

1.4.2 1D Critical Systems

The 1D Heisenberg spin chain is critical; in this and other such systems the entanglement entropy is known to scale as [12, 13, 14]

$$S^{\mathrm{vN}}_{\mathrm{PBC}} = \frac{c}{3}\ln(x') + s_1 \qquad S^{\mathrm{vN}}_{\mathrm{OBC}} = \frac{c}{6}\ln(2x') + \ln(g) + \frac{s_1}{2} \tag{1.7}$$

for systems with open (OBC) and periodic boundary conditions (PBC), where c is the central charge from conformal field theory, g is a universal boundary term [15], and s_1 is a model dependent constant. x' is the conformal mapping for the number of sites included in region A, used to account for the finite size of the Heisenberg chains, since (1.7) applies in the long chain-length limit. $x \to x' = (L/\pi)\sin(\pi x/L)$ for PBC and $x \to 2x'$ for OBC, where L is the length of the chain. This known scaling is used to verify the accuracy of our entanglement measurements in Chapter 3.

1.4.3 Subleading Corrections to the Area Law

Topological Entanglement Entropy

In systems exhibiting topological order – a type of order not, characterized by local order parameters, in which the degeneracy of the ground state depends on the topology of the system – there exists a universal subleading correction to the area law scaling of entanglement entropy called the *topological entanglement entropy*. For 2D systems with topological order, the entanglement entropy is known to scale as [11, 16]

$$S_{\mathrm{A}} = \alpha\ell - n\gamma + \mathcal{O}(1/\ell), \tag{1.8}$$

where ℓ is the length of the boundary, γ is the topological entanglement entropy, and n is related to the shape of the boundary. This topological entanglement entropy is zero when the system is not topologically ordered, and otherwise takes a value related to the degeneracy of the ground state. Thus it can be thought of as a type of topological order parameter. By measuring the entanglement entropy of regions of a system with certain geometries which are chosen to cancel out other terms of the entanglement scaling, it is possible to measure the topological entanglement entropy of a system [17].

At Quantum Critical Points

The scaling of entanglement entropy at quantum critical points is also known to hold information about universal quantities. In critical systems the area law scaling has universal additive logarithmic corrections [18, 19, 20]. By extracting these corrections, entanglement entropy can be used to to detect and characterize phase transitions.

1.5 Measurement of Entanglement Entropy

Many methods have been developed that are capable of measuring the entanglement entropy. In 1D density matrix renormalization group (DMRG) simulations and exact diagonalization are particularly powerful tools. They provide direct access to the wavefunction of a system. However exact diagonalization scales exponentially poorly as a function of system size and DMRG is primarily useful for 1D and multi-leg ladders. To study and extract these universal quantities in 2D and higher it is necessary to be able to measure entanglement entropy in a scalable type of simulation. Quantum Monte Carlo simulations scale well in any dimension and allow a choice of basis. In this thesis we explore methods of measuring entanglement entropy using quantum Monte Carlo simulations in the valence bond basis.

Chapter 2

Quantum Monte Carlo in the Valence Bond Basis

The numerical technique used in this research is valence bond quantum Monte Carlo (VB QMC) [21, 22]. Other commonly used lattice Monte Carlo techniques, such as the Stochastic Series Expansion [23] or world line [24] methods typically use the S^z basis, but VB QMC takes advantage of the unique properties of the valence bond basis.

In this chapter we introduce the valence bond basis, showing how it is used to represent singlet states. We then explain ground state projection, the method employed by VB QMC to get from a trial state to the ground state of our system. Next we discuss the Hamiltonian of our system, writing it in terms of "bond operators" that act on valence bond states. Finally we describe three different VB QMC algorithms: the single projector method, the double projector method, and the loop algorithm.

2.1 The Valence Bond Basis

The valence bond basis is a basis of states in which all sites are paired up into "valence bonds" (discussed further in Section 2.1.2). This basis can be used to represent any singlet state, i.e. any state with total spin equal to zero [25, 26]. In this section we introduce the spin-1/2 singlet state and its representation in terms of valence bonds. We then discuss some of the properties of the valence bond basis, and we conclude by examining the measurement of the inner product in the valence bond basis.

2.1.1 The Spin-1/2 Singlet State

Typically the states of spin-1/2 particles are represented in the S^z basis, the basis of eigenstates of the S^z operator ($\{|\uparrow\rangle, |\downarrow\rangle\}$ for one spin).

$$S^z|\uparrow\rangle = +\frac{1}{2}|\uparrow\rangle \qquad\qquad S^z|\downarrow\rangle = -\frac{1}{2}|\downarrow\rangle \tag{2.1}$$

A singlet state refers to a spin state of a particle or group of particles with vanishing total spin angular momentum. For two spin-1/2 particles (labeled here as a and b) there is exactly one singlet state, represented in the S^z basis and graphically as

$$\tfrac{1}{\sqrt{2}}\big(|\uparrow_a\downarrow_b\rangle - |\downarrow_a\uparrow_b\rangle\big) \quad = \quad$$

To establish notation which will be used later, we can go through the process of finding the eigenstates of the S^2 operator explicitly for two spin-1/2 particles. We begin by expressing the S^2 operator in terms of its different spin components:

$$\begin{aligned} S^2 &= (S^x)^2 + (S^y)^2 + (S^z)^2 && (2.2)\\ (S_a + S_b)^2 &= (S_a^x + S_b^x)^2 + (S_a^y + S_b^y)^2 + (S_a^z + S_b^z)^2 \\ &= (S^x \otimes \mathbb{1} + \mathbb{1} \otimes S^x)^2 + (S^y \otimes \mathbb{1} + \mathbb{1} \otimes S^y)^2 + (S^z \otimes \mathbb{1} + \mathbb{1} \otimes S^z)^2 && (2.3) \end{aligned}$$

where $\mathbb{1}$ is the 2x2 identity matrix and in Eq. (2.3) the operators are single spin operators. Switching to matrix notation now, we have

$$\begin{aligned} (S_a + S_b)^2 &= \left(\frac{1}{2}\begin{bmatrix} 0 & 1 \\ 1 & 0 \end{bmatrix} \otimes \begin{bmatrix} 1 & 0 \\ 0 & 1 \end{bmatrix} + \frac{1}{2}\begin{bmatrix} 1 & 0 \\ 0 & 1 \end{bmatrix} \otimes \begin{bmatrix} 0 & 1 \\ 1 & 0 \end{bmatrix}\right)^2 \\ &\quad + \left(\frac{1}{2}\begin{bmatrix} 0 & -i \\ i & 0 \end{bmatrix} \otimes \begin{bmatrix} 1 & 0 \\ 0 & 1 \end{bmatrix} + \frac{1}{2}\begin{bmatrix} 1 & 0 \\ 0 & 1 \end{bmatrix} \otimes \begin{bmatrix} 0 & -i \\ i & 0 \end{bmatrix}\right)^2 && (2.4) \\ &\quad + \left(\frac{1}{2}\begin{bmatrix} 1 & 0 \\ 0 & -1 \end{bmatrix} \otimes \begin{bmatrix} 1 & 0 \\ 0 & 1 \end{bmatrix} + \frac{1}{2}\begin{bmatrix} 1 & 0 \\ 0 & 1 \end{bmatrix} \otimes \begin{bmatrix} 1 & 0 \\ 0 & -1 \end{bmatrix}\right)^2 \\ &= \begin{bmatrix} 2 & 0 & 0 & 0 \\ 0 & 1 & 1 & 0 \\ 0 & 1 & 1 & 0 \\ 0 & 0 & 0 & 2 \end{bmatrix} && (2.5) \end{aligned}$$

where the eigenvalues and eigenvectors of (2.5) are:

$$\begin{aligned} &\lambda_1 = 2, && \mathbf{v}_1 = \begin{bmatrix} 1 & 0 & 0 & 0 \end{bmatrix}^\dagger && = |\uparrow\uparrow\rangle \\ &\lambda_2 = 2, && \mathbf{v}_2 = \begin{bmatrix} 0 & 0 & 0 & 1 \end{bmatrix}^\dagger && = |\downarrow\downarrow\rangle \\ &\lambda_3 = 2, && \mathbf{v}_3 = \tfrac{1}{\sqrt{2}}\begin{bmatrix} 0 & 1 & 1 & 0 \end{bmatrix}^\dagger && = \tfrac{1}{\sqrt{2}}\big(|\uparrow\downarrow\rangle + |\downarrow\uparrow\rangle\big) \\ &\lambda_4 = 0, && \mathbf{v}_4 = \tfrac{1}{\sqrt{2}}\begin{bmatrix} 0 & 1 & -1 & 0 \end{bmatrix}^\dagger && = \tfrac{1}{\sqrt{2}}\big(|\uparrow\downarrow\rangle - |\downarrow\uparrow\rangle\big). \end{aligned} \tag{2.6}$$

There is only one state with total spin equal to zero. The other three states have total spin 1. (If $|\psi\rangle$ is a total spin eigenstate then $S^2|\psi\rangle = s(s+1)|\psi\rangle$, where s is the total spin.)

2.1.2 Equivalence of the valence bond and the singlet state

A bond between two atoms created by sharing valence electrons in the outer orbitals is called a valence bond, or a covalent bond [27, 28]. Since electrons are fermionic (have half integer spin) their total wave function must be antisymmetric (an exchange of the identical particles in the wave function gives a factor of -1, i.e. $\Psi(a,b) = -\Psi(b,a)$). The total wave function is a product of the spatial and spin wave functions, so one of those wave functions must be antisymmetric and the other symmetric (an exchange of particles yields the same wave function, i.e. $\Psi(a,b) = \Psi(b,a)$). As part of the same valence bond, two electrons will have a spatially symmetric wave function, so their spin state must be antisymmetric. For two spin 1/2 particles the only antisymmetric spin state is the singlet state. Hence, in the case of two spin 1/2 particles, a valence bond is equivalent to the spin-1/2 singlet state.

We represent these valence bonds, or singlet states, in three ways:

- in the S^z basis using up spins and down spins, i.e. $\frac{1}{\sqrt{2}}\big(|\uparrow_a\downarrow_b\rangle - |\downarrow_a\uparrow_b\rangle\big)$,
- as a list of the bonded sites, i.e. $|(a,b)\rangle$,
- or pictorially as a bond joining two sites. 

A valence bond is a maximally entangled state; the entanglement between sites a and b is $S_a^{\text{vN}} = \ln(2)$. To illustrate this point, we can calculate the von Neumann entanglement entropy of the state $|\psi\rangle = \cos(\alpha)|\uparrow_a\downarrow_b\rangle + \sin(\alpha)|\downarrow_a\uparrow_b\rangle$.

$$\begin{aligned}\rho &= |\psi\rangle\langle\psi| && (2.7)\\ &= \cos^2(\alpha)|\uparrow_a\downarrow_b\rangle\langle\uparrow_a\downarrow_b| + \cos(\alpha)\sin(\alpha)|\uparrow_a\downarrow_b\rangle\langle\downarrow_a\uparrow_b| \\ &\qquad + \sin(\alpha)\cos(\alpha)|\downarrow_a\uparrow_b\rangle\langle\uparrow_a\downarrow_b| + \sin^2(\alpha)|\downarrow_a\uparrow_b\rangle\langle\downarrow_a\uparrow_b| && (2.8)\end{aligned}$$

$$\begin{aligned}\rho_a &= \text{Tr}_b(\rho) = \langle\uparrow_b|\rho|\uparrow_b\rangle + \langle\downarrow_b|\rho|\downarrow_b\rangle && (2.9)\\ &= \cos^2(\alpha)|\uparrow_a\rangle\langle\uparrow_a| + \sin^2(\alpha)|\downarrow_a\rangle\langle\downarrow_a| && (2.10)\end{aligned}$$

$$S_a^{\text{vN}} = -\text{Tr}(\rho_a \ln \rho_a) = -\cos^2(\alpha)\ln\big(\cos^2(\alpha)\big) - \sin^2(\alpha)\ln\big(\sin^2(\alpha)\big) \qquad (2.11)$$

The resulting entanglement entropy in Figure 2.1. Figure 2.2 shows higher order Renyi entropies for the same system.

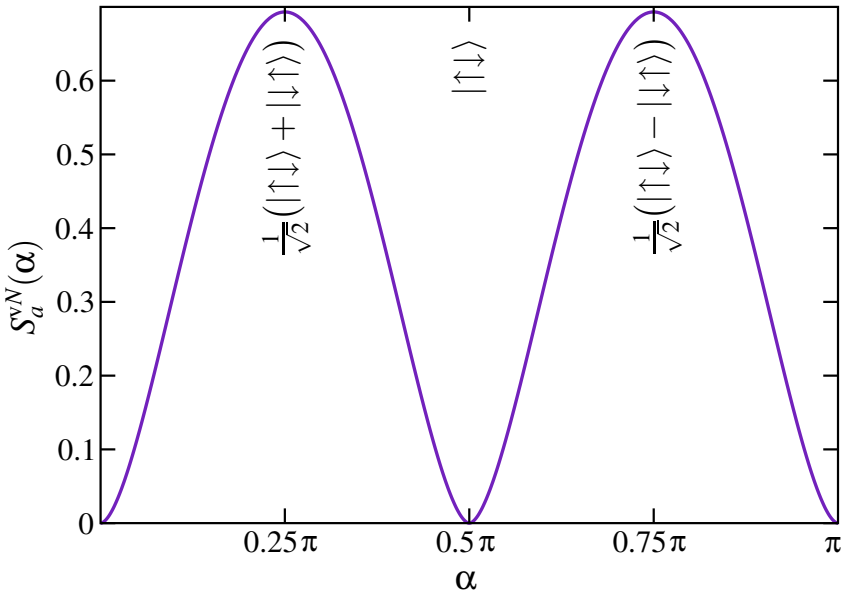

Figure 2.1: The von Neumann entanglement entropy for a two-site state $|\psi\rangle = \cos(\alpha)|\uparrow\downarrow\rangle + \sin(\alpha)|\downarrow\uparrow\rangle$. $|\psi\rangle$ is maximally entangled in the singlet state and one of the triplet states, and unentangled when the state is separable.

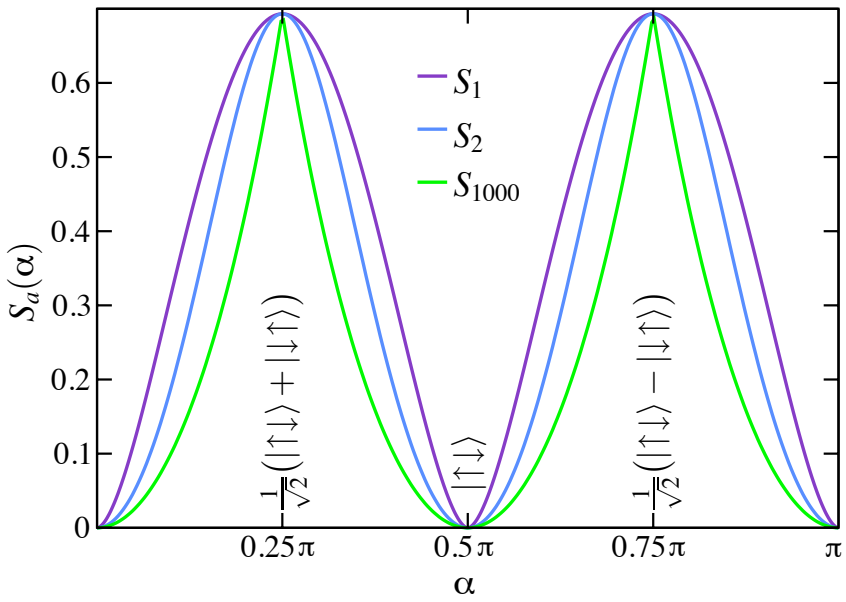

Figure 2.2: The von Neumann entanglement entropy (S_1), and the 2$^{\text{nd}}$ and 1000$^{\text{th}}$ Renyi entropies for a two-site state $|\psi\rangle = \cos(\alpha)|\uparrow\downarrow\rangle + \sin(\alpha)|\downarrow\uparrow\rangle$. All Renyi entropies take the same value for maximally and minimally entangled states.

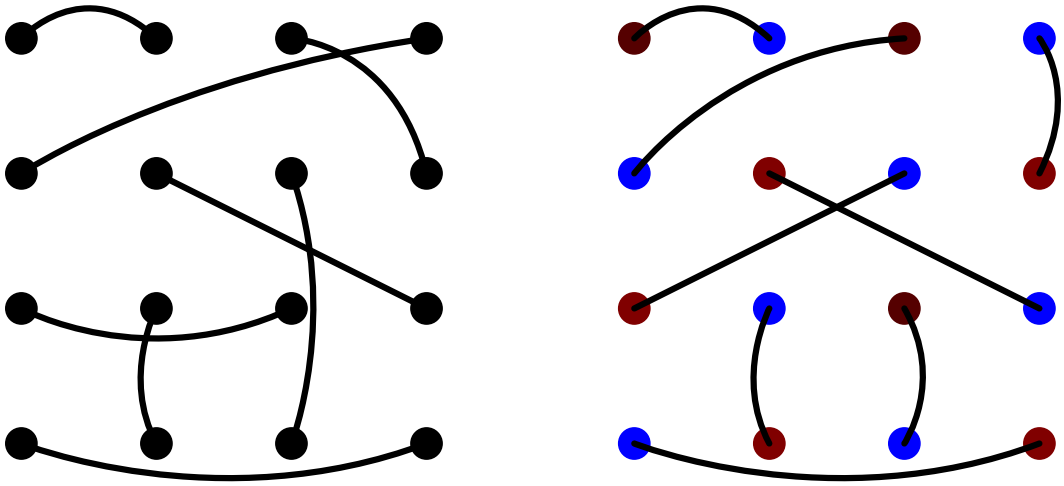

Figure 2.3: Two examples of valence bond coverings. (Left) An unrestricted valence bond state. (Right) Sites belonging to sublattice A are indicated in red and sublattice B sites are blue. This state only has bonds going from sites on sublattice A to sites on sublattice B.

2.1.3 Basis Properties

A collection of sites on a lattice can be paired into valence bonds such that each site belongs to exactly one bond. (See Fig. 2.3.) We call this a valence bond covering or valence bond state, and it is most conveniently represented as a list of sites that are paired in valence bonds:

$$|V\rangle = |(i_1, j_1)(i_2, j_2)\cdots(i_N, j_N)\rangle, \tag{2.12}$$

where bonds go from sites i to j for a lattice with $2N$ sites. Changing the order of the bonds in this list will not change the state, but reversing the order of an i, j pair will change the sign of the state.

For a system with an even number of spins, a basis of valence bond coverings can be used to represent an arbitrary singlet state, but in general that representation is not unique. The number of possible singlet states for a given number of spin-1/2 sites can be enumerated using the rule for the addition of angular momenta for each added spin,

$$S \otimes \tfrac{1}{2} = \left(S - \tfrac{1}{2}\right) \oplus \left(S + \tfrac{1}{2}\right), \tag{2.13}$$

where S is the $(2S+1)$-degenerate state of spin S [29].

$$\begin{aligned}
\tfrac{1}{2}\otimes\tfrac{1}{2} &= 0\oplus 1\\
\tfrac{1}{2}\otimes\tfrac{1}{2}\otimes\tfrac{1}{2} &= \tfrac{1}{2}\oplus\tfrac{1}{2}\oplus\tfrac{3}{2}\\
\tfrac{1}{2}\otimes\tfrac{1}{2}\otimes\tfrac{1}{2}\otimes\tfrac{1}{2} &= 0\oplus 0\oplus 1\oplus 1\oplus 1\oplus 2\\
\tfrac{1}{2}\otimes\tfrac{1}{2}\otimes\tfrac{1}{2}\otimes\tfrac{1}{2}\otimes\tfrac{1}{2} &= \tfrac{1}{2}\oplus\tfrac{1}{2}\oplus\tfrac{1}{2}\oplus\tfrac{1}{2}\oplus\tfrac{1}{2}\oplus\tfrac{3}{2}\oplus\tfrac{3}{2}\oplus\tfrac{3}{2}\oplus\tfrac{3}{2}\oplus\tfrac{5}{2}\\
\tfrac{1}{2}\otimes\tfrac{1}{2}\otimes\tfrac{1}{2}\otimes\tfrac{1}{2}\otimes\tfrac{1}{2}\otimes\tfrac{1}{2} &= \underbrace{0\oplus\cdots\oplus 0}_{5\text{ times}}\oplus\underbrace{1\oplus\cdots\oplus 1}_{9\text{ times}}\oplus\underbrace{2\oplus\cdots\oplus 2}_{5\text{ times}}\oplus 3
\end{aligned}$$

And for an arbitrary number of spins, 2N, the number of singlet states is given by [29]

$$C^N_{\text{sing}} = \frac{1}{N+1}\binom{2N}{N} = \frac{(2N)!}{N!(N+1)!}, \tag{2.14}$$

In contrast, the number of possible valence bond states (for 2N sites) is given by

$$C^N_{\text{VB}} = \frac{(2N)!}{2^N N!}, \tag{2.15}$$

since we choose sites at random ($2N!$ ways to choose them) pairing them, but the order in which each member of the bond is chosen does not matter (divide by 2 for every bond), nor does the order in which the N bonds are chosen (divide by $N!$). For $N > 1$ there are more valence bond coverings than singlet states, the excess increasing drastically with increasing N (see Figure 2.4).

The valence bond states are nonorthogonal and overcomplete. Because of this overcompleteness we can eliminate some of the valence bond states and still represent any singlet state. In fact, this can be seen for a four-site system by again diagonalizing the S^2 matrix. This time we will only look at the $S^z = 0$ sector, since all the singlet states will be found there. With the same method used to get (2.5), we find:

$$S^2_{\text{reduced}} = \begin{bmatrix} 2 & 1 & 1 & 1 & 1 & 0\\ 1 & 2 & 1 & 1 & 0 & 1\\ 1 & 1 & 2 & 0 & 1 & 1\\ 1 & 1 & 0 & 2 & 1 & 1\\ 1 & 0 & 1 & 1 & 2 & 1\\ 0 & 1 & 1 & 1 & 1 & 2 \end{bmatrix} \begin{array}{ll} \lambda_1 = 6, & \mathbf{v_1} = \begin{bmatrix} 1 & 1 & 1 & 1 & 1 & 1 \end{bmatrix}\\ \lambda_2 = 2, & \mathbf{v_2} = \begin{bmatrix} 1 & 0 & 0 & 0 & 0 & -1 \end{bmatrix}\\ \lambda_3 = 2, & \mathbf{v_3} = \begin{bmatrix} 0 & 1 & -3 & 3 & -1 & 0 \end{bmatrix}\\ \lambda_4 = 2, & \mathbf{v_4} = \begin{bmatrix} 0 & 3 & 1 & -1 & -3 & 0 \end{bmatrix}\\ \lambda_5 = 0, & \mathbf{v_5} = \begin{bmatrix} 0 & 1 & -1 & -1 & 1 & 0 \end{bmatrix}\\ \lambda_6 = 0, & \mathbf{v_6} = \begin{bmatrix} 1 & -1 & 0 & 0 & -1 & 1 \end{bmatrix} \end{array} \tag{2.16}$$

where $\mathbf{v_5}$ and $\mathbf{v_6}$ are the (so far unnormalized) singlet states. Note that there are only two singlet states, while there are three valence bond states for a four-site system. And, interestingly, the four-site singlet states are composed of two two-site singlet states. Expressing

$\mathbf{v_5}$ and $\mathbf{v_6}$ in the spin and valence bond basis we get

$$\mathbf{v_5} = \frac{1}{2}\Big(|\downarrow\uparrow\downarrow\uparrow\rangle - |\downarrow\uparrow\uparrow\downarrow\rangle - |\uparrow\downarrow\downarrow\uparrow\rangle + |\uparrow\downarrow\uparrow\downarrow\rangle\Big) = |(a,b)(c,d)\rangle \tag{2.17}$$

$$\mathbf{v_6} = \frac{1}{2}\Big(|\downarrow\downarrow\uparrow\uparrow\rangle - |\downarrow\uparrow\uparrow\downarrow\rangle - |\uparrow\downarrow\downarrow\uparrow\rangle + |\uparrow\uparrow\downarrow\downarrow\rangle\Big) = |(a,d)(c,b)\rangle \tag{2.18}$$

$\mathbf{v_5} =$ 

$\mathbf{v_5} =$ 

Since $\mathbf{v_5}$ and $\mathbf{v_6}$ are degenerate eigenstates, we could have also chosen one of them to be the other valence bond state, $|(a,c)(b,d)\rangle$, or some linear combination of any of the three possible valence bond states.

It is convenient to define two sublattices, A and B, on a bipartite lattice, such that sites on sublattice A are neighbored only by sublattice B sites and vice versa. (See Figure 2.3.) We can choose the valence bond coverings containing only bonds between the two sublattices. This restriction eliminates some, though not all, of the overcompleteness of the valence bond states. The now-reduced number of valence bond states is simply $C^N_{\mathrm{AB}} = N!$ for a system of $2N$ spins.

One way to see the linear dependence of the remaining valence bond states would be to again diagonalize the S^2 matrix, for a six-site system this time (in which there are $3! = 6$ A-B sublattice valence bond states, but only $6!/(3!4!) = 5$ singlet states). This, however, would require us to diagonalize a 20x20 matrix if we only look at the $S^z = 0$ sector.

Another way to see the linear dependence of the A-B sublattice states is to look at the overlap matrix, that is a matrix filled with the inner products between the different states, i.e.

$$\begin{aligned}
|\psi_1\rangle &= |(a,d)(c,f)(e,b)\rangle \\
|\psi_2\rangle &= |(a,d)(c,b)(e,f)\rangle \\
|\psi_3\rangle &= |(a,b)(c,f)(e,d)\rangle \\
|\psi_4\rangle &= |(a,f)(c,b)(e,d)\rangle \\
|\psi_5\rangle &= |(a,b)(c,d)(e,f)\rangle \\
|\psi_6\rangle &= |(a,f)(c,d)(e,b)\rangle
\end{aligned}
\qquad
\mathcal{O} = \begin{bmatrix} \langle\psi_1|\psi_1\rangle & \cdots & \langle\psi_6|\psi_1\rangle \\ \vdots & \ddots & \vdots \\ \langle\psi_1|\psi_6\rangle & \cdots & \langle\psi_6|\psi_6\rangle \end{bmatrix} = \frac{1}{4}\begin{bmatrix} 4 & 2 & 2 & 1 & 1 & 2 \\ 2 & 4 & 1 & 2 & 2 & 1 \\ 2 & 1 & 4 & 2 & 2 & 1 \\ 1 & 2 & 2 & 4 & 1 & 2 \\ 1 & 2 & 2 & 1 & 4 & 2 \\ 2 & 1 & 1 & 2 & 2 & 4 \end{bmatrix}$$

If the overlap matrix $\mathcal{O}$ is put in reduced row echelon form we can see that it only takes

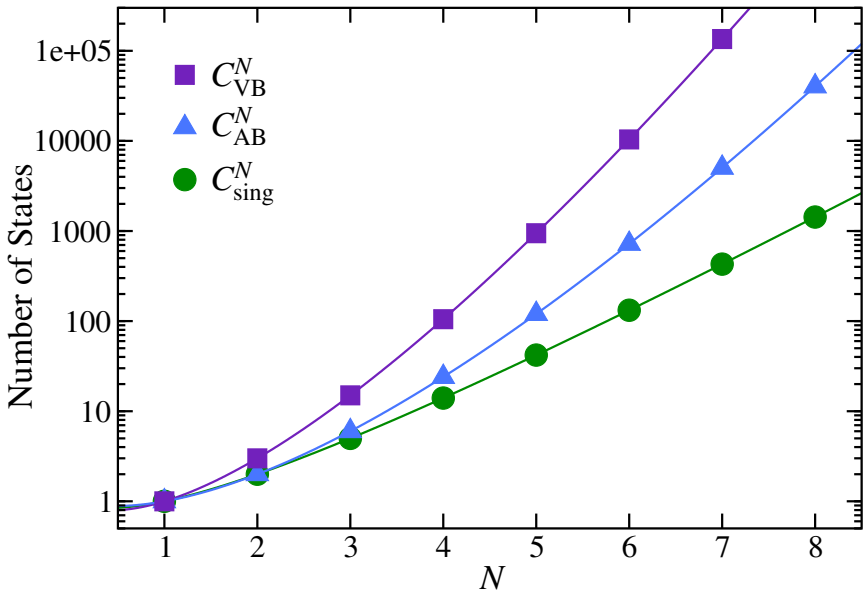

Figure 2.4: The number of singlet states $C^N_{\rm sing}$, valence bond states $C^N_{\rm VB}$, and valence bond states restricted to A-B sublattice bonds $C^N_{\rm AB}$, for a system of $2N$ spins.

five of the six vectors to span the space of six site singlet states.

$$\mathcal{O}_{rre} = \begin{bmatrix} 1 & 0 & 0 & 0 & 0 & 1 \\ 0 & 1 & 0 & 0 & 0 & -1 \\ 0 & 0 & 1 & 0 & 0 & -1 \\ 0 & 0 & 0 & 1 & 0 & 1 \\ 0 & 0 & 0 & 0 & 1 & 1 \\ 0 & 0 & 0 & 0 & 0 & 0 \end{bmatrix} \qquad |\psi_6\rangle = |\psi_1\rangle - |\psi_2\rangle - |\psi_3\rangle + |\psi_4\rangle + |\psi_5\rangle \tag{2.19}$$

Also the last state can be written as a linear combination of the other five states. It is possible to choose a set of linearly independent states by putting the sites in a circular configuration and eliminating any state with valence bonds crossing each other. The resulting set of linearly independent states corresponds exactly to the singlet basis [29].

2.1.4 The Inner Product

In the S^z basis, to calculate the overlap between two states we simply take the inner products between the various terms of the two states. Since the S^z basis states are all mutually orthonormal, the process is quite simple, for example:

$$|\psi\rangle = \frac{1}{2}\big(\sqrt{3}|\uparrow\uparrow\rangle + |\downarrow\downarrow\rangle\big) \qquad |\phi\rangle = \frac{1}{\sqrt{2}}\big(|\downarrow\uparrow\rangle + |\downarrow\downarrow\rangle\big)$$

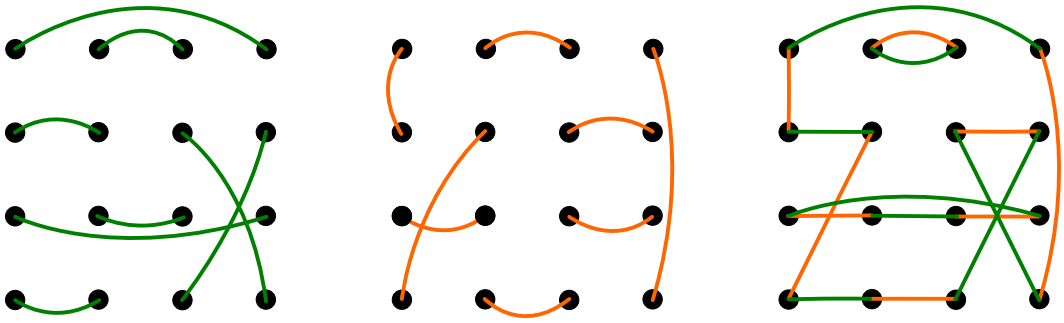

Figure 2.5: Calculation of the inner product between the states $|V^{\mathrm{L}}\rangle$ and $|V^{\mathrm{R}}\rangle$. The inner product is simply $\langle V^{\mathrm{L}}|V^{\mathrm{R}}\rangle = 2^{(N_{\mathrm{loops}}-N_{\mathrm{sites}}/2)}$, where N_{loops} is the number of loops created by overlapping the two valence bond states. In this case there are 3 loops and 16 sites, so $\langle V^{\mathrm{L}}|V^{\mathrm{R}}\rangle = 2^{-5}$.

$$\begin{aligned}\langle\psi|\phi\rangle &= \frac{1}{2\sqrt{2}}\big(\sqrt{3}\langle\uparrow\uparrow|\downarrow\uparrow\rangle + \sqrt{3}\langle\uparrow\uparrow|\downarrow\downarrow\rangle + \langle\downarrow\downarrow|\downarrow\uparrow\rangle + \langle\downarrow\downarrow|\downarrow\downarrow\rangle\big)\\ &= \frac{1}{2\sqrt{2}}\big(0+0+0+1\big) = \frac{1}{2\sqrt{2}}\end{aligned} \tag{2.20}$$

We can compute valence bond state overlaps in the same way, by expressing the states in the S^z basis. From (2.17) and (2.18) we have:

$$\begin{aligned}\langle\mathbf{v_5}|\mathbf{v_6}\rangle &= \frac{1}{4}\big(\langle\downarrow\uparrow\downarrow\uparrow|\downarrow\downarrow\uparrow\uparrow\rangle - \langle\downarrow\uparrow\downarrow\uparrow|\downarrow\uparrow\uparrow\downarrow\rangle - \langle\downarrow\uparrow\downarrow\uparrow|\uparrow\downarrow\downarrow\uparrow\rangle + \langle\downarrow\uparrow\downarrow\uparrow|\uparrow\uparrow\downarrow\downarrow\rangle\\ &\quad -\langle\downarrow\uparrow\uparrow\downarrow|\downarrow\downarrow\uparrow\uparrow\rangle + \langle\downarrow\uparrow\uparrow\downarrow|\downarrow\uparrow\uparrow\downarrow\rangle + \langle\downarrow\uparrow\uparrow\downarrow|\uparrow\downarrow\downarrow\uparrow\rangle - \langle\downarrow\uparrow\uparrow\downarrow|\uparrow\uparrow\downarrow\downarrow\rangle\\ &\quad -\langle\uparrow\downarrow\downarrow\uparrow|\downarrow\downarrow\uparrow\uparrow\rangle + \langle\uparrow\downarrow\downarrow\uparrow|\downarrow\uparrow\uparrow\downarrow\rangle + \langle\uparrow\downarrow\downarrow\uparrow|\uparrow\downarrow\downarrow\uparrow\rangle - \langle\uparrow\downarrow\downarrow\uparrow|\uparrow\uparrow\downarrow\downarrow\rangle\\ &\quad +\langle\uparrow\downarrow\uparrow\downarrow|\downarrow\downarrow\uparrow\uparrow\rangle - \langle\uparrow\downarrow\uparrow\downarrow|\downarrow\uparrow\uparrow\downarrow\rangle - \langle\uparrow\downarrow\uparrow\downarrow|\uparrow\downarrow\downarrow\uparrow\rangle + \langle\uparrow\downarrow\uparrow\downarrow|\uparrow\uparrow\downarrow\downarrow\rangle\big)\\ &= \frac{1}{4}\left(\langle\downarrow\uparrow\uparrow\downarrow|\downarrow\uparrow\uparrow\downarrow\rangle + \langle\uparrow\downarrow\downarrow\uparrow|\uparrow\downarrow\downarrow\uparrow\rangle\right) = \frac{1}{2}.\end{aligned} \tag{2.21}$$

since all other terms will vanish. This method of calculating the inner product, however, quickly becomes intractable even with a small number of spins. A more intuitive way to calculate the overlap is to superimpose diagrams of the two valence bond states, as in Figure 2.5. We can rewrite the valence bond states from the figure, keeping the bonds belonging to the same loop together. Bonds from separate loops will have no overlap with each other.

$$\begin{aligned}|V_{\mathrm{L}}\rangle &= |(1,4)(3,2)(6,5)(8,15)(9,12)(11,10)(14,13)(16,7)\rangle\\ &= |(1,4)(16,7)(8,15)(14,13)(6,5)\rangle \otimes |(3,2)\rangle \otimes |(9,12)(11,10)\rangle \qquad (2.22)\\ |V_{\mathrm{R}}\rangle &= |(1,5)(3,2)(6,13)(8,7)(9,10)(11,12)(14,15)(16,4)\rangle\\ &= |(16,4)(8,7)(14,15)(6,13)(1,5)\rangle \otimes |(3,2)\rangle \otimes |(11,12)(9,10)\rangle \qquad (2.23)\end{aligned}$$

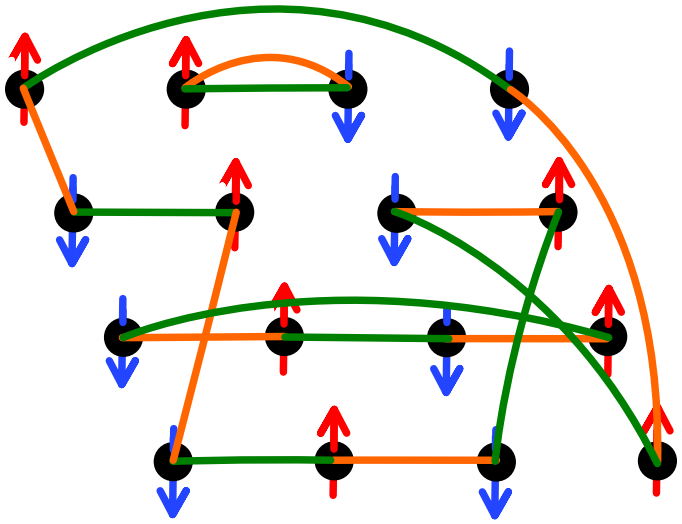

Figure 2.6: A possible spin state satisfying the loop configuration from Figure 2.5. There are two compatible spin states for each loop.

Each set of sites is in a state consisting of a sum (including some negative terms) over a subset of all possible combinations of spins, such that there is an equal number of up and down spins in each state. This set is restricted by the valence bonds; if there is a bond going between sites a and b then the spin on site a must always be opposite of the spin on site b.

Examining the third loop, which contains four sites, for the state of $|V_{\mathrm{L}}\rangle$ sites 9 and 12 must always have opposite spins, as must sites 10 and 11. There are six $S^z = 0$ states, four of which satisfy these restrictions. For the state of $|V_{\mathrm{R}}\rangle$ there are also four spin states that satisfy its restrictions, but since the restrictions are different (spins 11 and 12 are opposite and spins 9 and 10 are opposite) it turns out that when we overlap $|V_{\mathrm{L}}\rangle$ and $|V_{\mathrm{R}}\rangle$ there are only two spin states that satisfy both sets of restrictions. This is true for all loops; there are only two possible spin states. These states correspond to alternating up and down spins around the loop, or equivalently, the state in which all the sublattice A sites in the loop have a given spin (up or down) and the sublattice B sites have the opposite spin.

The number of S^z spin states needed to express a valence bond state (for a system of N spins) is $2^{N/2}$, since $\big(|\uparrow\downarrow\rangle - |\downarrow\uparrow\rangle\big)^{\otimes N/2}$ gives $2^{N/2}$ distinct N-spin states. The inner product

can be expressed as a product of the inner products for each of the loops:

$$\begin{aligned}\langle V^{\mathrm{L}}|V^{\mathrm{R}}\rangle &= \prod_{k=1}^{N_{\mathrm{loops}}} \frac{1}{\sqrt{2^{N_k^s/2}}}\Big(\langle\alpha_1| + \langle\alpha_2| + \cdots \langle\alpha_{2^{N_k^s/2}}|\Big)\frac{1}{\sqrt{2^{N_k^s/2}}}\Big(|\beta_1\rangle + |\beta_2\rangle + \cdots |\beta_{2^{N_k^s/2}}\rangle\Big) \\ &= \prod_{k=1}^{N_{\mathrm{loops}}} \frac{1}{2^{N_k^s/2}}\Big(2\Big) = \left(\frac{1}{2^{N_{\mathrm{sites}}/2}}\right) 2^{N_{\mathrm{loops}}} = 2^{N_{\mathrm{loops}}-N_{\mathrm{sites}}/2}, \end{aligned} \tag{2.24}$$

where N_k^s is the number of spins contained in loop k, and the $|\alpha_i\rangle$'s and $|\beta_i\rangle$'s are the spin states used to represent $|V^{\mathrm{L}}\rangle$ and $|V^{\mathrm{R}}\rangle$ respectively. There are exactly two non-vanishing terms in the inner product for each loop. If not for the A-B sublattice convention (see Figure 2.3) it would be possible to get negative overlaps between states. A maximal value of the overlap can be obtained through the inner product of a state with itself. Then there are $N/2$ loops, one for every two sites. There are $2^{N/2}$ compatible spin configurations, and the overlap is exactly its maximal value, 1.

The inner product can be used to calculate the expectation values of observables, normalize states, and as a factor in the Monte Carlo weights, all necessary for quantum Monte Carlo algorithms in the valence bond basis, as we discuss in upcoming sections.

2.2 Ground State Projection

Quantum Monte Carlo in the valence bond basis is a ground state projection technique, which means we start with a trial wave function and apply a high power of the Hamiltonian so we are left with the ground state of the system.

We can represent any singlet state as a linear combination of valence bond states:

$$|\psi\rangle = \sum_r f_r|(a_1^r, b_1^r), (a_2^r, b_2^r), \ldots, (a_{N/2}^r, b_{N/2}^r)\rangle = \sum_r f_r|V^r\rangle, \tag{2.25}$$

but due to the overcompleteness of even the A-B sublattice valence bond basis, this representation is not unique. However, we can represent this state uniquely in terms of energy eigenstates of a Hamiltonian,

$$|\psi\rangle = \sum_n c_n|n\rangle, \tag{2.26}$$

where $|n\rangle$ is the n^{th} energy eigenstate of a Hamiltonian and the c_n's are the unique coefficients.

If we apply the Hamiltonian to the state in Eq. (2.26) we are left with

$$\mathcal{H}|\psi\rangle = \sum_n c_n\mathcal{H}|n\rangle = \sum_n c_nE_n|n\rangle = c_0E_0|0\rangle + c_1E_1|1\rangle + c_2E_2|2\rangle + \cdots, \tag{2.27}$$

where E_n is the n^{th} energy eigenvalue of the Hamiltonian, $\mathcal{H}$. We can then take out a factor of E_0 to get

$$\mathcal{H}|\psi\rangle = E_0 \left(c_0|0\rangle + c_1 \frac{E_1}{E_0}|1\rangle + c_2 \frac{E_2}{E_0}|2\rangle + \cdots \right). \tag{2.28}$$

If E_0 is the energy largest in magnitude, then the magnitude of the coefficients of the excited states are all fractions less than 1. In that case, if we apply the Hamiltonian a large number of times, denoted by m, all terms excluding the ground state term will vanish.

$$\mathcal{H}^m|\psi\rangle = E_0^m \left(c_0|0\rangle + c_1 \left(\frac{E_1}{E_0}\right)^m |1\rangle + c_2 \left(\frac{E_2}{E_0}\right)^m |2\rangle + \cdots \right) \approx E_0^m c_0|0\rangle \tag{2.29}$$

If the ground state energy is not the largest in magnitude, as is the case with the Heisenberg model, we can manipulate the Hamiltonian slightly by adding or subtracting an appropriately chosen constant term, x, in which case we will have

$$(\mathcal{H} - x)^m|\psi\rangle = (E_0 - x)^m \left(c_0|0\rangle + c_1 \left(\frac{E_1 - x}{E_0 - x}\right)^m |1\rangle + \cdots \right) \approx (E_0 - x)^m c_0|0\rangle. \tag{2.30}$$

We are left with a state proportional to the ground state of the system, provided the initial state $|\psi\rangle$ has some non-zero overlap with the ground state. Fortunately, every valence bond state has non-zero overlap with every other valence bond state. Ground state projection is used in valence bond quantum Monte Carlo, but it is also the basis of many other numerical algorithms such as Lanczos [30], diffusion quantum Monte Carlo [31], and Green's function Monte Carlo [32].

2.3 The Hamiltonian and Bond Operators

Throughout this thesis we study systems in one and two dimensions, which are described by the isotropic, antiferromagnetic Heisenberg Hamiltonian,

$$\mathcal{H}_{\text{Heis}} = J \sum_{\langle i,j \rangle} \mathbf{S}_i \cdot \mathbf{S}_j = J \sum_{\langle i,j \rangle} \left(S_i^z S_j^z + \tfrac{1}{2} \left[S_i^+ S_j^- + S_i^- S_j^+ \right] \right), \tag{2.31}$$

where the coupling constant J is always positive, and $\sum_{\langle i,j \rangle}$ represents a sum over all nearest-neighbor pairs of sites. This Hamiltonian favors antiparallel spins and will flip pairs of antiparallel spins.

We slightly modify the Hamiltonian in order to facilitate the ground state projection scheme:

$$\mathcal{H} = \left(\mathcal{H}_{\text{Heis}} - \sum_{\langle i,j \rangle} \tfrac{1}{4} \right) = \sum_{\langle i,j \rangle} \left(\mathbf{S}_i \cdot \mathbf{S}_j - \tfrac{1}{4} \right) = - \sum_{\langle i,j \rangle} H_{ij}. \tag{2.32}$$

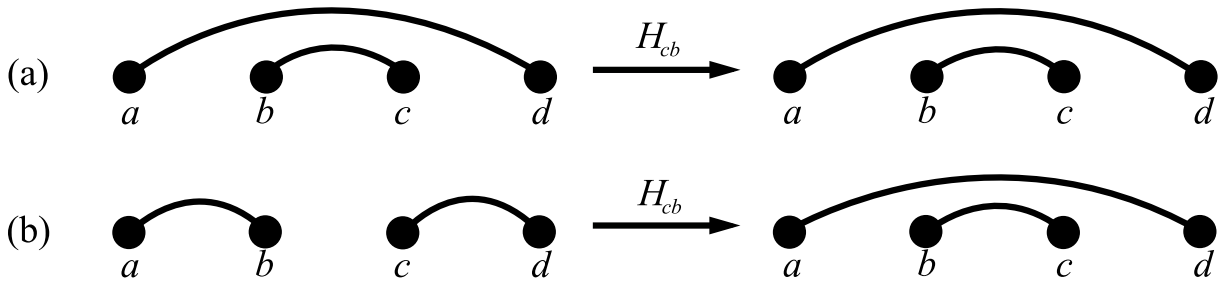

Figure 2.7: Bond operator H_{cb} acting on four-site states. (a) The sites c and b are already joined by a valence bond, so the bond operator does nothing. (b) Sites c and b are not joined, so H_{cb} acts to join them. The new valence bond state gets a factor of $\frac{1}{2}$.

Here the coupling constant J is set to 1, and we rewrite the Hamiltonian in terms of a list of *bond operators,* H_{ij}, where $H_{ij} = -\left(\mathbf{S}_i \cdot \mathbf{S}_j - \frac{1}{4}\right)$.

The effect of these bond operators acting on a valence bond basis state is surprisingly simple. If a bond operator acts on two sites already joined by a valence bond, it acts as the identity and does not change the state. If the two sites acted upon are not joined in a valence bond, the operator joins those two sites. As a byproduct the two sites that were once joined to those sites form a valence bond themselves, and the resulting state gains a factor of 1/2. This is depicted in Figure 2.7 and will be shown mathematically, but first let us examine the effect of bond operators on a general spin-1/2 state.

We can rewrite the dot product of spin operators:

$$\mathbf{S}_i \cdot \mathbf{S}_j = \tfrac{1}{2}\left[(S_i + S_j)^2 - S_i^2 - S_j^2\right], \tag{2.33}$$

however, the $(S_i + S_j)^2$ operator has two different eigenvalues (0 and 2) or, if the initial state is not one of the four total spin eigenstates, applying this operator will change the state.

Acting with a bond operator on an eigenstate of total spin for two spins yields:

$$H_{ij}|\psi\rangle = \begin{cases} -\left(\frac{1}{2}\left[(0) - \frac{3}{4} - \frac{3}{4}\right] - \frac{1}{4}\right)|\psi\rangle = |\psi\rangle & \text{for total spin 0} \\ -\left(\frac{1}{2}\left[(2) - \frac{3}{4} - \frac{3}{4}\right] - \frac{1}{4}\right)|\psi\rangle = 0 & \text{for total spin 1} \end{cases} \tag{2.34}$$

If we want to use the bond operators on valence bond basis states, Eq. (2.34) tells us what happens when sites i and j are already joined in a valence bond, but we still need to look at the case in which the sites are initially part of two different valence bonds. For four sites a, b, c, and d, with sites a and c on sublattice A and the others on sublattice B, we apply the operator H_{cb} to a valence bond state.

$$\begin{aligned} H_{cb}|(a,b)(c,d)\rangle &= H_{cb}\tfrac{1}{\sqrt{2}}\big(|\uparrow_a\downarrow_b\rangle - |\downarrow_a\uparrow_b\rangle\big)\tfrac{1}{\sqrt{2}}\big(|\uparrow_c\downarrow_d\rangle - |\downarrow_c\uparrow_d\rangle\big) \\ &= \tfrac{1}{2}H_{cb}\big(|\uparrow_a\downarrow_d\rangle|\uparrow_c\downarrow_b\rangle - |\uparrow_a\uparrow_d\rangle|\downarrow_c\downarrow_b\rangle - |\downarrow_a\downarrow_d\rangle|\uparrow_c\uparrow_b\rangle + |\downarrow_a\uparrow_d\rangle|\downarrow_c\uparrow_b\rangle\big) \end{aligned}$$

At this point it is convenient to represent the spin states involving sites b and c in terms of eigenvalues of singlet and triplet states.

$$\begin{aligned} H_{cb}|(a,b)(c,d)\rangle &= \tfrac{1}{2}H_{cb}\left(|\uparrow_a\downarrow_d\rangle\tfrac{1}{\sqrt{2}}\left[\tfrac{1}{\sqrt{2}}\big(|\uparrow_c\downarrow_b\rangle - |\downarrow_c\uparrow_b\rangle\big) + \tfrac{1}{\sqrt{2}}\big(|\uparrow_c\downarrow_b\rangle + |\downarrow_c\uparrow_b\rangle\big)\right]\right) \\ &\quad -\tfrac{1}{2}H_{cb}\Big(|\uparrow_a\uparrow_d\rangle|\downarrow_c\downarrow_b\rangle + |\downarrow_a\downarrow_d\rangle|\uparrow_c\uparrow_b\rangle\Big) \\ &\quad -\tfrac{1}{2}H_{cb}\left(|\downarrow_a\uparrow_d\rangle\tfrac{1}{\sqrt{2}}\left[\tfrac{1}{\sqrt{2}}\big(|\uparrow_c\downarrow_b\rangle - |\downarrow_c\uparrow_b\rangle\big) - \tfrac{1}{\sqrt{2}}\big(|\uparrow_c\downarrow_b\rangle + |\downarrow_c\uparrow_b\rangle\big)\right]\right) \end{aligned} \tag{2.35}$$

We are left with states for which we know the outcome of applying this bond operator. The states with a nonzero total spin will vanish.

$$\begin{aligned} H_{cb}|(a,b)(c,d)\rangle &= \tfrac{1}{2}\left(|\uparrow_a\downarrow_d\rangle\tfrac{1}{\sqrt{2}}\left[\tfrac{1}{\sqrt{2}}\big(|\uparrow_c\downarrow_b\rangle - |\downarrow_c\uparrow_b\rangle\big)\right]\right) \\ &\qquad -\tfrac{1}{2}\left(|\downarrow_a\uparrow_d\rangle\tfrac{1}{\sqrt{2}}\left[\tfrac{1}{\sqrt{2}}\big(|\uparrow_c\downarrow_b\rangle - |\downarrow_c\uparrow_b\rangle\big)\right]\right) \\ &= \tfrac{1}{2}\left[\tfrac{1}{\sqrt{2}}\big(|\uparrow_a\downarrow_d\rangle - |\downarrow_a\uparrow_d\rangle\big)\right]\left[\tfrac{1}{\sqrt{2}}\big(|\uparrow_c\downarrow_b\rangle - |\downarrow_c\uparrow_b\rangle\big)\right] \\ &= \tfrac{1}{2}|(a,d)(c,b)\rangle \end{aligned} \tag{2.36}$$

As was asserted earlier, the operator acts to rearrange the bonds, and the state gains a factor of $\frac{1}{2}$. If not for the subtraction of $\frac{1}{4}$ from the Hamiltonian (2.32), applying the bond operators would be much more complicated, yielding superpositions of valence bond states, causing a "branching" algorithm. Additionally, we would be left with non-singlet states, due to the change in Equation (2.34). This fact, that the application of bond operators to a valence bond basis state yields another basis state state with finite overlap between those states, and all other basis states makes these operators ideal for use in a Monte Carlo algorithm.

2.4 The Monte Carlo Algorithm

In Section 2.2 we saw that applying a high power of the Hamiltonian to any initial state possessing some overlap with the ground state will give us a state proportional to the ground state of the system. However, computing this exactly would be extremely computationally expensive. The Hamiltonian has N_{nn} terms, one for each possible nearest-neighbor bond. Raising it to the even power m would give us $(N_{nn})^m$ terms each containing m bond operators,

$$\mathcal{H}^m = \left(\sum_{k=1}^{N_{nn}} H_k\right)^m = \sum_{k_1=1}^{N_{nn}}\sum_{k_2=1}^{N_{nn}}\cdots\sum_{k_m=1}^{N_{nn}}\left(H_{k_1}H_{k_2}\cdots H_{k_m}\right) = \sum_{r=1}^{(N_{nn})^m} P_r, \tag{2.37}$$

where k goes over each of the possible nearest neighbor bonds, and P_r is the r^{th} possible list of m bond operators. Applying $\mathcal{H}^m$ to a trial state $|V\rangle$ gives us

$$\mathcal{H}^m|V\rangle = \sum_{r=1}^{(N_{nn})^m} P_r|V\rangle = \sum_{r=1}^{(N_{nn})^m} W_r|V_r\rangle = \sum_{r=1}^{(N_{nn})^m} 2^{-m_r^{\text{off}}}|V_r\rangle, \tag{2.38}$$

where W_r, the weight, is the product of the factors of $\frac{1}{2}$ gained by applying off-diagonal bond operators to the trial state. The ratio of weights is used in Monte Carlo sampling to determine whether to keep a given configuration.

Instead of computing the full sum from (2.38), we stochastically sample terms from the sum, sampling proportional to their weight W_r in the sum. In the "single projector" method (Section 2.4.1) we project only one valence bond state, but are limited in the observables we can then calculate. The "double projector" method (Section 2.4.2) projects two separate states, which can then be used to find expectation values of various operators. The loop algorithm (Section 2.4.3) is an improvement on the double projector algorithm.

2.4.1 Single Projector

The first of the valence bond quantum Monte Carlo algorithms, the single projector method was conceived by Anders Sandvik in 2005 [21]. This algorithm projects one trial state into the ground state of the system by applying lists of m bond operators to that state. The result of applying these bond operators is a new state and a weight, as in (2.38). Every Monte Carlo step a few (q) of the bond operators in the list are changed randomly. (We change $q = 3$ bond operators at each step.) The new list of bond operators is applied to the trial state and the weights are compared. If the new weight is larger than the weight from the previous step, the changes in the bond operator list are kept and a measurement can be made. Otherwise, the new state is kept with the probability equal to the ratio of the new and old weights:

$$\text{Prob(keep)} = \frac{W_{\text{new}}}{W_{\text{old}}}. \tag{2.39}$$

If the new state is not kept, the changes to the bond operator list are undone, and a measurement can be made, but the measurement is on the old state, the state generated by the previous bond operator list. In this way, the states are sampled according to their relative weight in the ground state wavefunction. The process of changing the bond operator list and deciding whether to keep the changes is continued. Each repetition is considered one Monte Carlo step. The full algorithm is shown below:

1. Choose or generate an initial valence bond state $|V\rangle$.

2. Generate a list of m random bond operators P_{old}.

3. Apply the list of bond operators to the initial state.
$$P_{\text{old}}|V\rangle = W_{\text{old}}|V_{\text{old}}\rangle$$

4. Copy P_{old} to P_{new} and randomly change a predetermined number, q, of the bond operators in P_{new}.

5. Apply the new list of bond operators to the original initial state.
$$P_{\text{new}}|V\rangle = W_{\text{new}}|V_{\text{new}}\rangle$$

6. Generate a random number $A \in [0, 1)$.

7. If $A < W_{\text{new}}/W_{\text{old}}$, relabel all "new" quantities as "old".

8. Take a measurement using the state $|V_{\text{old}}\rangle$.

9. Go to Step 4.

Measurements

In the single projector method we can measure the ground state energy using a reference state $|\Psi\rangle$:

$$E_0 = \frac{\langle\Psi|\mathcal{H}_{\text{Heis}}|0\rangle}{\langle\Psi|0\rangle} = \frac{\sum_r \langle\Psi|\mathcal{H}_{\text{Heis}}P_r|V\rangle}{\sum_r \langle\Psi|P_r|V\rangle} = \frac{\sum_r W_r\langle\Psi|\mathcal{H}_{\text{Heis}}|V_r\rangle}{\sum_r W_r\langle\Psi|V_r\rangle} \tag{2.40}$$

At this point we can put in our expression for the Heisenberg Hamiltonian from (2.32).

$$E_0 = \frac{\sum_r W_r\langle\Psi|\left(-\sum_{k=1}^{N_{nn}}(H_k + \frac{1}{4})\right)|V_r\rangle}{\sum_r W_r\langle\Psi|V_r\rangle} \tag{2.41}$$

If we choose the reference state to be a classical Néel state (spins alternating over the sites, i.e. $|\uparrow\downarrow\uparrow\downarrow\cdots\uparrow\downarrow\uparrow\downarrow\rangle$) which has equal overlap with every valence bond state ($\langle\Psi_{\text{Néel}}|V_r\rangle = 2^{-N/2}$ for a system of N sites) we can further simplify this formula,

$$E_0 = -\sum_{k=1}^{N_{nn}} \frac{\sum_r W_r\langle\Psi_{\text{Néel}}|H_k|V_r\rangle + \sum_r W_r\langle\Psi_{\text{Néel}}|\frac{1}{4}|V_r\rangle}{\sum_r W_r\langle\Psi_{\text{Néel}}|V_r\rangle} = -\left\langle\sum_{k=1}^{N_{nn}} 2^{o_k}\right\rangle - \frac{N_{nn}}{4}, \tag{2.42}$$

where o_k is 1 for an off-diagonal operator (acting on sites not already joined by a valence bond) and 0 otherwise. We can rewrite this in terms of the number of diagonal n_{diag} and off-diagonal n_{off} operators in the Hamiltonian and use the fact that $n_{\text{diag}} + n_{\text{off}} = N_{nn}$,

$$E_0 = -\left\langle \frac{n_{\text{off}}}{2} + n_{\text{diag}} \right\rangle - \frac{N_{nn}}{4} = -\frac{1}{2}\left(\langle n_{\text{diag}} \rangle + N_{nn} \right) \tag{2.43}$$

One way to measure this is to count the number of nearest neighbor valence bonds in every state we measure, since there will be a diagonal term in the Hamiltonian for every nearest neighbor bond. This method is exact in the limits $m \to \infty$ and the number of states sampled $\to \infty$. It is also possible to measure $\langle n_{\text{diag}} \rangle$ by counting the number of diagonal bond operators in the operator list P_r at each step, and it is exact in the limit $m \to \infty$.

It is important to note that this energy measurement is not variational, and as such can give results lower than the ground state energy. However, the energy measurement with the double projector method, described below, is variational and approaches the ground state energy from above.

This algorithm is not limited to measuring the ground state energy; we can measure other operators for which the ground state is an eigenstate. It also is possible to add in one triplet state and measure the singlet-triplet gap [21]. And we can measure properties of the valence bonds, like the bond length distribution or the valence bond entanglement entropy, introduced in the next chapter.

2.4.2 Double Projector

The double projector method was also included in the original valence bond quantum Monte Carlo paper by Anders Sandvik [21]. The main difference between the double and single projector methods is that in the double projector method, as the name implies, we project two states into the ground state. That is, we are propagating two different lists of bond operators; though the trial state for each list of bond operators can be the same. (We refer to these as the left and right lists of bond operators.) This allows us to measure the expectation value of any operator that can act on a valence bond state, not just the Hamiltonian.

The sampling weights in this scheme are also different, including the overlap between the two projected states. The weight for each pair of states is:

$$W_{\text{total}} = W^L W^R \langle V^L | V^R \rangle, \tag{2.44}$$

where W^L and W^R are $2^{-m_{\text{off}}}$ (the factors of $\frac{1}{2}$ accrued by applying off-diagonal bond operators) for the left and right operators lists respectively.

The algorithm is as follows:

1. Choose or generate an initial valence bond state $|V\rangle$.

2. Generate two lists of m random bond operators L_{old} and R_{old} .

3. Apply the lists of bond operators to the initial state.
$$\langle V|L^{\dagger}_{\text{old}} = W^{L}_{\text{old}}\langle V^{L}_{\text{old}}| \qquad R_{\text{old}}|V\rangle = W^{R}_{\text{old}}|V^{R}_{\text{old}}\rangle$$

4. Copy L_{old} to L_{new} and randomly change a predetermined number, q, of the bond operators in L_{new}.

5. Apply the new left list of bond operators to the original initial state.
$$\langle V|L^{\dagger}_{\text{new}} = W^{L}_{\text{new}}\langle V^{L}_{\text{new}}|$$

6. Generate a random number $A \in [0, 1)$.

7. If $A < W^{L}_{\text{new}}W^{R}_{\text{old}}\langle V^{L}_{\text{new}}|V^{R}_{\text{old}}\rangle / W^{L}_{\text{old}}W^{R}_{\text{old}}\langle V^{L}_{\text{old}}|V^{R}_{\text{old}}\rangle$, relabel all "new" left quantities as "old".

8. Copy R_{old} to R_{new} and randomly change a predetermined number, q, of the bond operators in R_{new}.

9. Apply the new right list of bond operators to the original initial state.
$$R_{\text{new}}|V\rangle = W^{R}_{\text{new}}|V^{R}_{\text{new}}\rangle$$

10. Generate a random number $A \in [0, 1)$.

11. If $A < W^{L}_{\text{old}}W^{R}_{\text{new}}\langle V^{L}_{\text{old}}|V^{R}_{\text{new}}\rangle / W^{L}_{\text{old}}W^{R}_{\text{old}}\langle V^{L}_{\text{old}}|V^{R}_{\text{old}}\rangle$, relabel all "new" right quantities as "old".

12. Take a measurement using the states $\langle V^{L}_{\text{old}}|$ and $|V^{R}_{\text{old}}\rangle$.

13. Go to Step 4.

Measurements

Using this double projector method the general expectation value an observable $\mathcal{O}$ is given by

$$\langle \mathcal{O} \rangle = \frac{\sum_{i,j} \langle V | L_i^\dagger \mathcal{O} R_j | V \rangle}{\sum_{i,j} \langle V | L_i^\dagger R_j | V \rangle} = \frac{\sum_{i,j} W_i^L W_j^R \langle V_i^L | \mathcal{O} | V_j^R \rangle}{\sum_{i,j} W_i^L W_j^R \langle V_i^L | V_j^R \rangle}. \tag{2.45}$$

We are already sampling states according to the weight from (2.44), so in this scheme we need to measure

$$\langle \mathcal{O} \rangle = \frac{\sum_{i,j} W_i^L W_j^R \langle V_i^L | V_j^R \rangle \frac{\langle V_i^L | \mathcal{O} | V_j^R \rangle}{\langle V_i^L | V_j^R \rangle}}{\sum_{i,j} W_i^L W_j^R \langle V_i^L | V_j^R \rangle} = \left\langle \frac{\langle V^L | \mathcal{O} | V^R \rangle}{\langle V^L | V^R \rangle} \right\rangle. \tag{2.46}$$

The double projector method is much more versatile in the range of observables that can be measured. In addition to anything that can be measured with the single projector method we can also measure the *Swap* operator, spin correlations functions, and, by adding triplet states into the mix, staggered magnetization, and spin stiffness, among other things [29]. In Chapter 4 this double projector algorithm is used the measure the expectation value of a *Swap* operator which enables the measurement of entanglement entropy.

2.4.3 Loop Algorithm

The double projector algorithm scales as $\max(m^2, Nm)$ for a list of m bond operators acting on an N-site system. Normally we use $m = cN$ for some $c > 1$. If we have $c < \frac{1}{2}$ it would not be possible to get a valence bond configuration entirely independent of the initial state. So most often the double projector algorithm scales as m^2. A significant improvement on this scaling was made in the loop algorithm, developed by Sandvik and Evertz in 2008 [33, 34], which scales as $\max(m, N)$.

The loop algorithm is similar to the double projector method, in that we are projecting two states, and we can use those to find inner products and expectations values. However, in this algorithm the bond operators are separated into their diagonal $H(1)$ and off-diagonal $H(2)$ parts,

$$H_{ab}(1) = \tfrac{1}{4} - S_a^z S_b^z \tag{2.47}$$

$$H_{ab}(2) = -\tfrac{1}{2}(S_a^+ S_b^- + S_a^- S_b^+). \tag{2.48}$$

We also keep track of one of the possible spin configurations of our system. For our chosen initial valence bond state(s) we pick a compatible spin configuration. The diagonal and

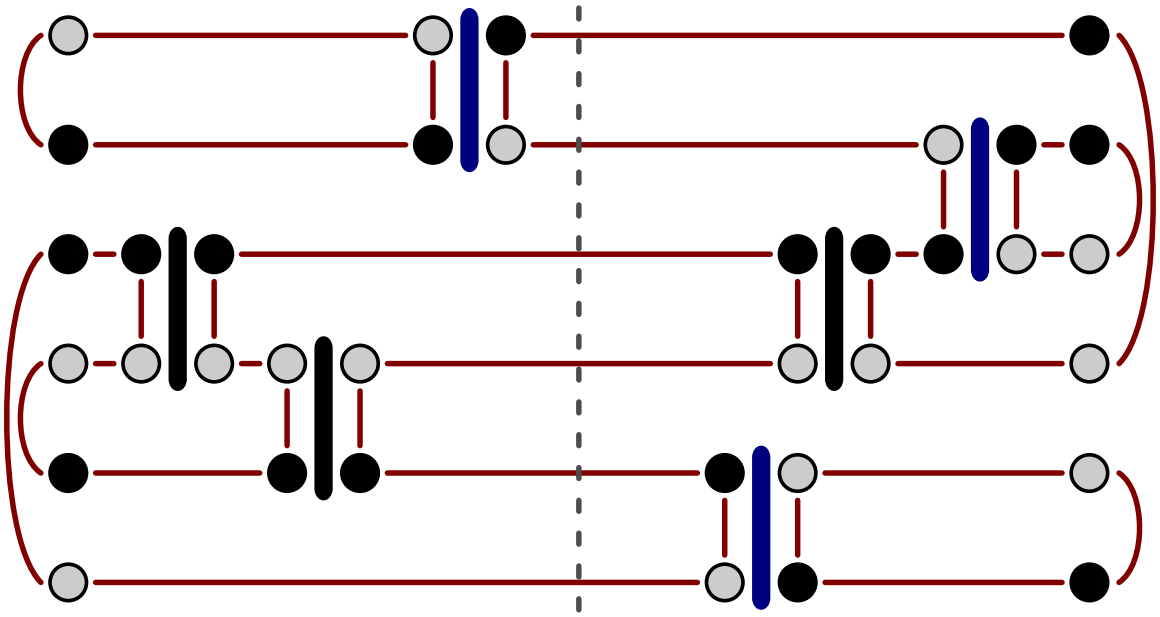

Figure 2.8: A valence bond-spin-operator configuration for the loop algorithm for 6-site system. There are $m = 3$ operators per operator list L and R. The dark (light) sites represent up (down) spins, and the black (blue) vertical bars are diagonal (off-diagonal) operators. The valence bond states and compatible spin states ($\langle V^L_{\text{init}}|$, $\langle Z^L|$) and ($|V^R_{\text{init}}\rangle$, $|Z^R\rangle$) are shown on the left and right edges of the diagram respectively. The dashed line down the middle is the point in between the two operators lists, where the propagated states $\langle V^L|$ and $|V^R\rangle$ lie.

off-diagonal bond operators can only act on nearest neighbor pairs of antiparallel spins. The off-diagonal operators flip the spins of the sites they act on, shown in Figure 2.8.

The loop algorithm is as follows:

1. Choose or generate initial valence bond states $|V^L_{\text{init}}\rangle$ and $|V^R_{\text{init}}\rangle$. (These can be chosen as the same state.)

2. Assign a spin to each of the sites such that the spin states $|Z^L\rangle$ and $|Z^R\rangle$ are compatible with the valence bonds.

3. Generate two lists of m diagonal bond operators L and R, ensuring operators only act on nearest neighbor pairs of antiparallel spins.

4. Generate loops from the operator configuration, as illustrated in Figure 2.8.

5. For each loop, flip all of the spins in that loop with probability $\frac{1}{2}$. This may cause some of the diagonal operators to become off-diagonal.

6. Take measurements.

7. Update each diagonal bond operator, placing it on a random antiparallel pair of nearest neighbor spins.

8. Go to step 4.

Measurements

We can return to the valence bond representation to take measurements using (2.46). Constructing the VB-loop-operator diagram in Step 4 of the algorithm gives us the projected valence bond configurations $\langle V^L| = \langle V^L_{\text{init}}|L^\dagger$ and $|V^R\rangle = R|V^R_{\text{init}}\rangle$. The number of loops in the overlap $\langle V^L|V^R\rangle$ is easily counted, as the number of distinct loops crossing the dividing line in the middle of the VB-loop-operator diagram. (See Figure 2.8.)

Chapter 3

Valence Bond Entanglement Entropy

Recently a new quantity called *valence bond entanglement entropy* (S^{VB}) was proposed [13, 35, 36], which seems to have properties similar to the von Neumann entanglement entropy (S^{vN}). The main advantage of S^{VB} is the simplicity of its measurement when working in the valence bond basis. For a valence bond basis state S^{VB} between two regions, A and B, it is defined as

$$S^{\mathrm{VB}}_{\mathrm{A}} = \ln(2)\mathcal{N}_{\mathrm{A}}, \tag{3.1}$$

where $\mathcal{N}_{\mathrm{A}}$ is the number of valence bonds crossing the boundary between regions A and B. (See Figure 3.1.)

S^{VB} shares some properties with S^{vN}; in particular, for both quantities $S_{\mathrm{A}} = S_{\mathrm{B}}$. Also, as with S^{vN}, $S^{\mathrm{VB}} = 0$ for systems with no entanglement between regions A and B. For any single valence bond basis state (not a superposition of valence bond states) S^{VB} and S^{vN} agree exactly. In one-dimensional Heisenberg spin-1/2 systems S^{VB} seems to be in good agreement with results from conformal field theory (CFT) for S^{vN} [35]. However, in two dimensions S^{VB} shows a multiplicative logarithmic correction to the area law for the isotropic Heisenberg model. Ground states of unfrustrated 2D spin-1/2 systems with exclusively nearest neighbour interactions are expected to follow an area law [10, 37], though until now there has been a lack of computational results confirming this.

To examine the correspondence of S^{VB} to a known measure of entanglement [38] we place our S^{VB} data alongside measurements of S^{vN} on the same system, calculated with density matrix renormalization group (DMRG) [39, 40] simulations by I. Gonzalez and R. Melko. S^{VB} is calculated using a single projector valence bond quantum Monte Carlo (VB QMC) scheme [22, 21].

In this chapter we begin by looking at the scaling of S^{VB} and S^{vN} for 1D systems with open (OBC) and with periodic boundary conditions (PBC), and we compare the value

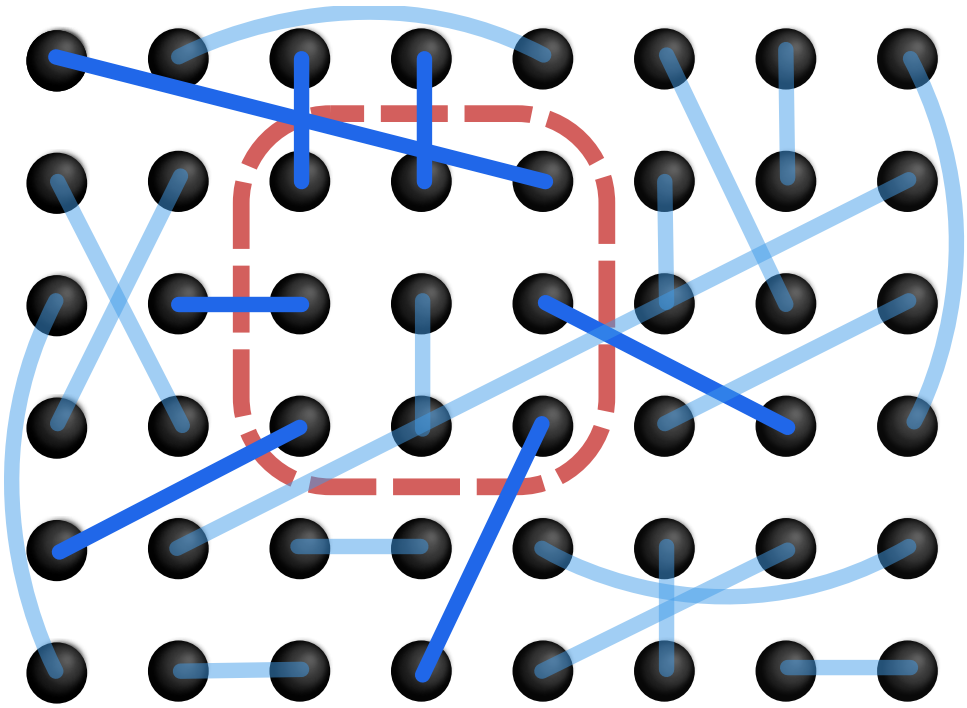

Figure 3.1: The valence bond entanglement entropy (3.1) between regions A and B of a valence bond basis state is defined as the number of valence bonds crossing between the two regions multiplied by a factor of $\ln(2)$. This diagram shows a state with $S_{\mathrm{A}}^{\mathrm{VB}} = 7\ln(2)$.

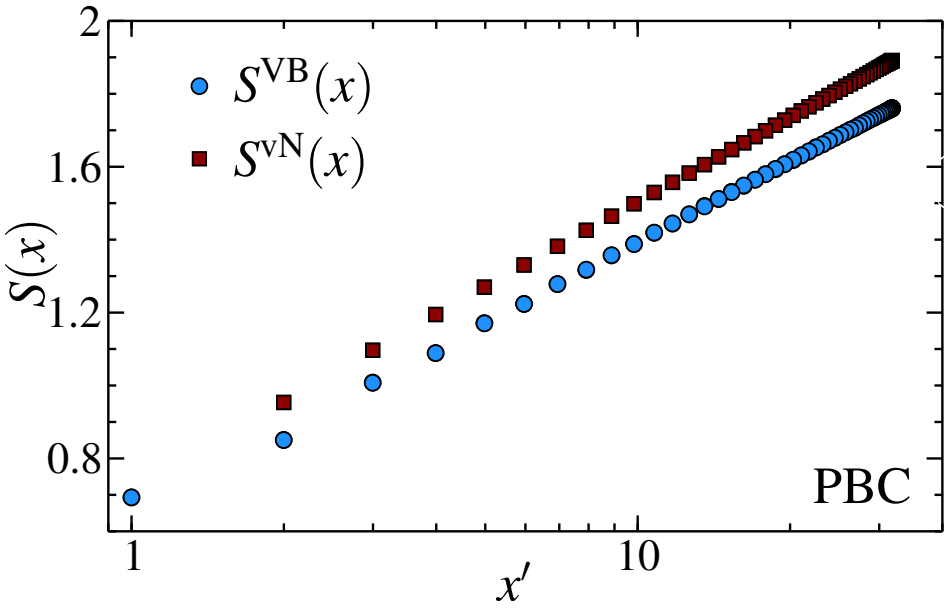

Figure 3.2: Entanglement entropies for a 1D Heisenberg chain with PBC and L=100 sites, as a function of the conformal distance $x' = (L/\pi)\sin(\pi x/L)$ [12].

of the conformal charge c to the expected value for this system. We then approach 2D, looking at M-leg ladder systems to determine the scaling of these entanglement entropies.

My contribution to this project was the measurement of all of the $S^{\rm VB}$ data using a single projector quantum Monte Carlo program, and the linear regression for the $S^{\rm VB}$ data.

3.1 One Dimensional Systems

We begin by simulating one dimensional systems, examining both the OBC and PBC cases. It is convenient to denote the size of region A by the number of sites included in that region (i.e. for a 1D system of length L, $S_{\rm A} = S(x)$ is the entanglement entropy for a system where region A contains sites $\{1, 2, \ldots, x\}$ and the remainder of the sites $\{x+1, x+2, \ldots, L\}$ belong to region B.

As mentioned in section 1.4.2, for a 1D critical system, such as the 1D Heisenberg spin chain, the scaling of the entanglement entropy is described by [12, 13, 14]

$$S^{\rm vN}_{\rm PBC} = \frac{c}{3}\ln(x') + s_1 \tag{3.2}$$

$$S^{\rm vN}_{\rm OBC} = \frac{c}{6}\ln(2x') + \ln(g) + \frac{s_1}{2} \tag{3.3}$$

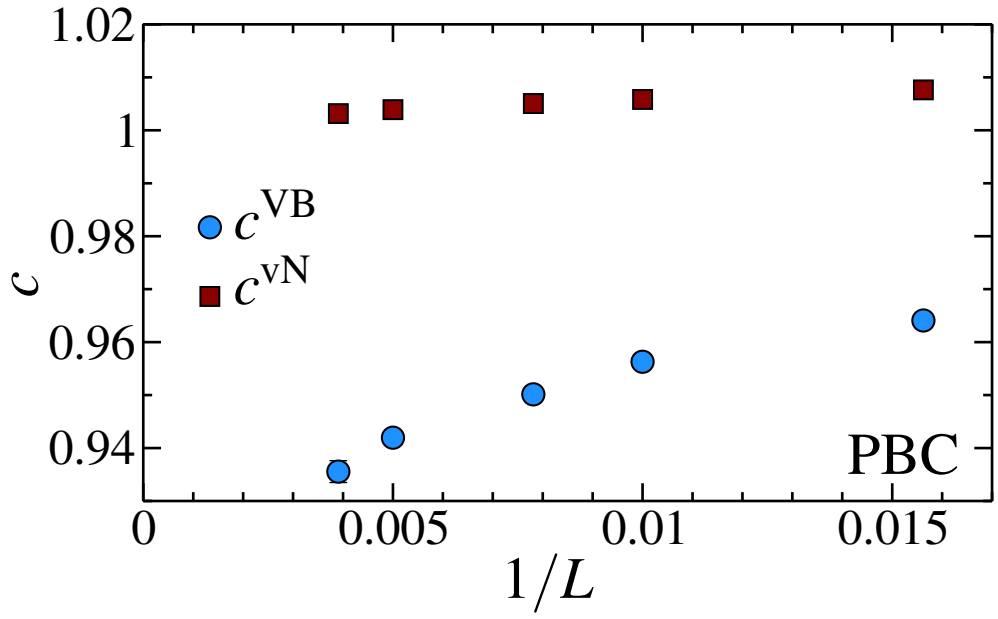

Figure 3.3: The central charge, c, found using linear regression fits of the entanglement entropy data for periodic Heisenberg chains for length L=64, 100, 128, 200, and 256. Data for the two smallest points ($S(1)$ and $S(L-1)$) are removed for the calculation of c.

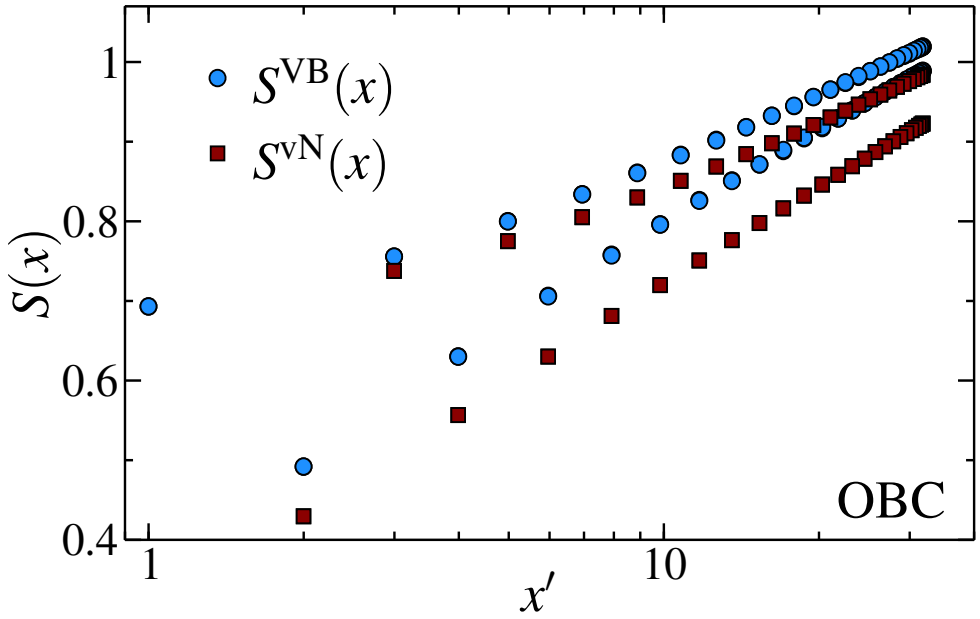

Figure 3.4: Entanglement entropies for a 1D 100-site Heisenberg chain with OBC as a function of the conformal distance $x' = (L/\pi)\sin(\pi x/L)$.

Figure 3.2 shows the S^{VB} measurements for a periodic spin chain of length $L = 100$ sites, plotted alongside S^{vN} data. S^{VB} seems to fit well to the expected scaling, though it is lower than S^{vN}. We use linear regression to fit the S^{VB} and S^{vN} data for several system sizes to Equation (3.2), and Figure 3.3 shows the results for the central charge c^{vN} approaching 1 (the expected value for this system [41]) as the system size increases, however c^{VB} approaches a lower value. It has been shown analytically [42], using the probability distribution for valence bonds connecting subsystems of a given length, that $c^{\mathrm{VB}} = \frac{12 \ln 2}{\pi^2} \approx 0.84 < c^{\mathrm{vN}}$.

For the 100-site OBC system (Figure 3.4), we see both S^{vN} and S^{VB} split into two branches, where the upper branch corresponds to an odd number of sites in region A, and the lower branch to an even number of sites. This branching is due to a "dimerization" effect caused by the open boundary conditions [13]. In contrast to the PBC case, S^{VB} is now higher than S^{vN} implying that, unlike the successive Renyi entropies, S^{VB} does not give a bound on S^{vN} . Figure 3.5 shows the linear regression fits of the lower branch of OBC data for several different system sizes to the first term of Equation (3.3). As the number of points included is decreased (until we are only using data where the division between regions A and B is "far" from the open boundaries of the system) we see c^{vN} approach a constant value for all system sizes. As the system size increases c^{vN} approaches the expected value of 1 [41]. On the other hand, from the S^{VB} data, it is not clear whether c^{VB} approaches a constant value for large system sizes. We see only that c^{VB} is lower than the expected value of 1 [36], and that it is lower than the c^{VB} value given by the PBC data.

3.2 Approaching Two Dimensions

We now move towards two dimensions by adding "legs" to our one dimensional OBC chains. Due to the constraints imposed by the DMRG on the geometry of region A the sites must be arranged in a snaking pattern (Fig 3.6). The DMRG data, to which we compare S^{VB}, are limited to ladders with $M = 7$ legs because of the poor scaling of the algorithm when approaching 2D. The VB QMC algorithm scales as Nm for a system with N sites [34], so we measure up to $M = 20$ with minimal CPU effort.

Figures 3.7 and 3.8 show the entanglement entropies for three- and four-leg ladders respectively. As with the 1D OBC spin chain, $S^{\mathrm{VB}} > S^{\mathrm{vN}}$ for these M-leg ladders. The entanglement entropies show different behavior depending on whether the number of legs is even or odd. Odd-leg ladders are gapless, and so all sites contribute to the entanglement, thus $S(x) \propto \ln(x')$ as in the 1D case [43]. Even-leg ladders have a spin gap and so only sites within the correlation length ξ from the boundary between A and B contribute to the entanglement, thus for even-leg ladders $S(x \gtrsim \xi) = \text{const}$. Both even- and odd-leg ladders split into branches, as shown in the figure insets, though the even-leg ladders have

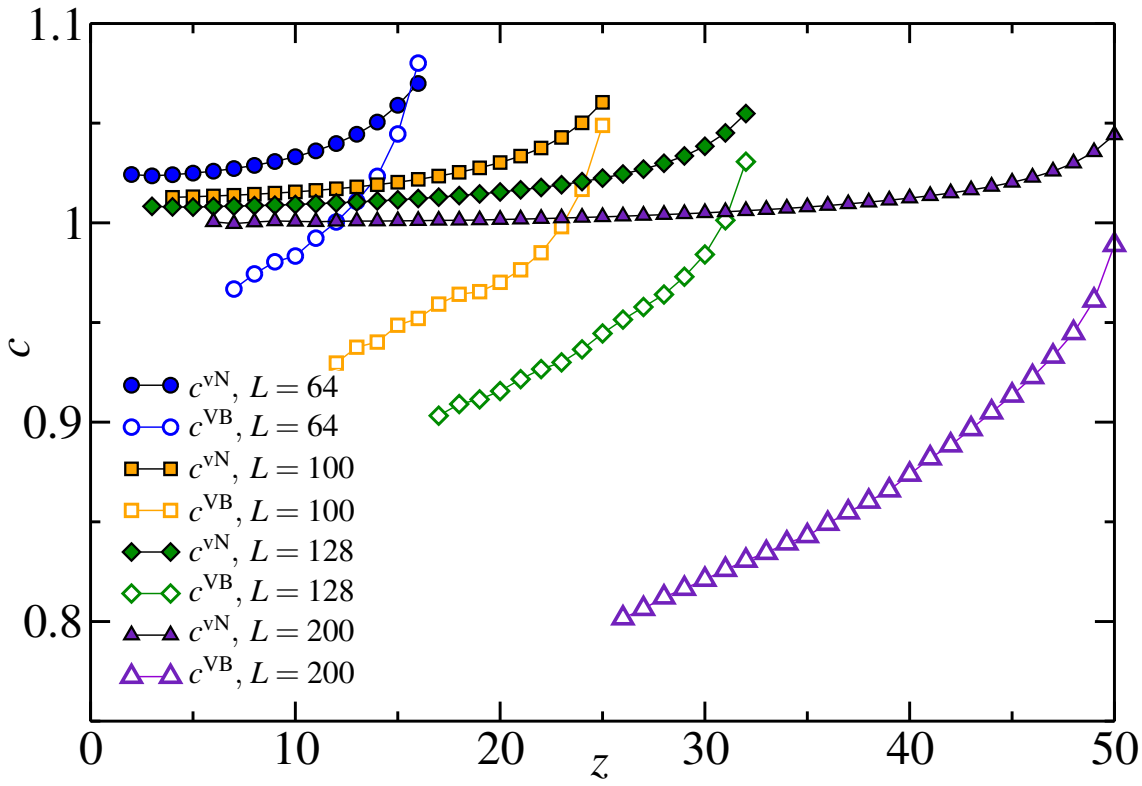

Figure 3.5: The central charge, c, for 1D OBC chains of lengths $L = 64$, 100, 128, and 200. The slope of the data depends on the number of points z included in the linear regression fit, as can be seen looking at 3.4. We fit the lower branch of the data, systematically decreasing z until there are too few points left to get an accurate fit.

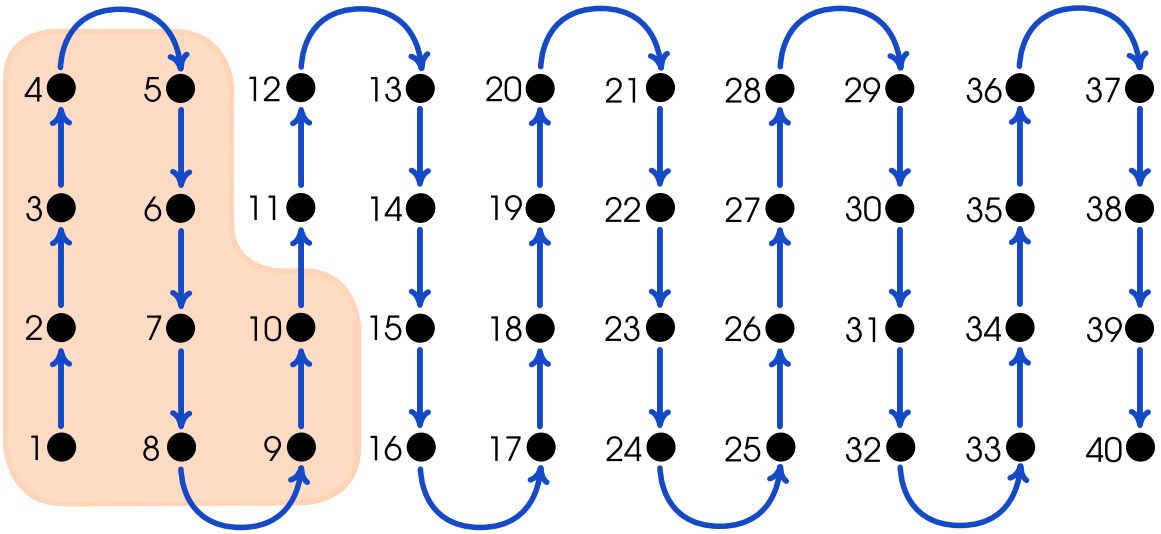

Figure 3.6: The site numbering scheme for a $M = 4$ leg ladder of length $L = 10$. Region A is the shaded area, and the entanglement entropy of this region is labelled by the largest site x in region A. In this case $x = 10$, and we would measure $S(10)$. This geometry is imposed by the DMRG, but we use the same configuration in the VB QMC.

a pattern with period M whereas the odd-leg ladder entanglement entropies have a period of $2M$.

3.3 The Area Law

Using these multileg ladders we can examine the adherence of the ground state of the 2D isotropic Heisenberg model to the area law. To do this we use M-leg ladders, including $2M^2$ sites within region A. This ensures that the boundary between regions A and B cuts cleanly across all the legs of the system so that the length of the boundary is proportional to M, while also keeping the dividing line between the two regions far enough from the open boundaries of the system to avoid boundary effects. Additionally, the 2:1 aspect ratio ensures that, even for odd-leg ladders, an even number of sites is included in region A, reducing the odd-even oscillations in the entanglement entropies.

In Figure 3.9 we plot the entanglement entropies $S(x)/M$ versus M, for M-leg ladders, on a logarithmic scale. If the scaling of the entanglement entropy follows an area law we should see $S(x)/M$ approach a constant value for large M. We include both systems with 100 sites per leg, and systems with $4M$ sites per leg. In the second case the size of region A is proportional to the size of the ladder, and the dividing line between regions A and B is always cutting the ladder through the middle.

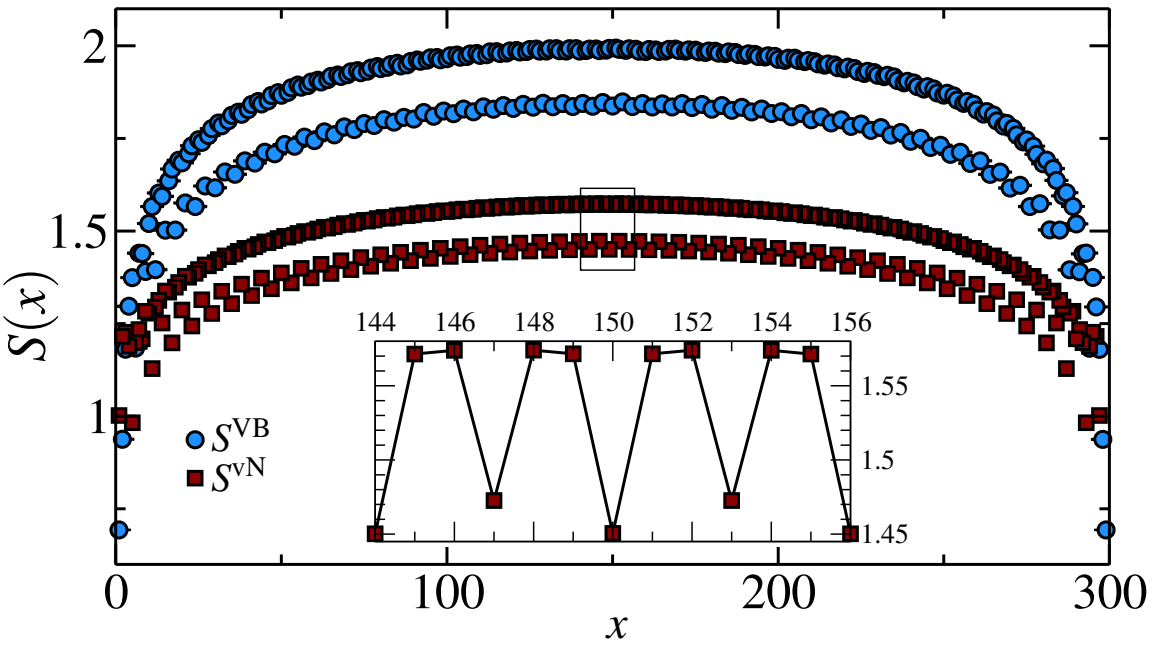

Figure 3.7: Entanglement entropies for a three-leg ladder with OBC and 100 sites per leg. The inset shows a close up view of the boxed region.

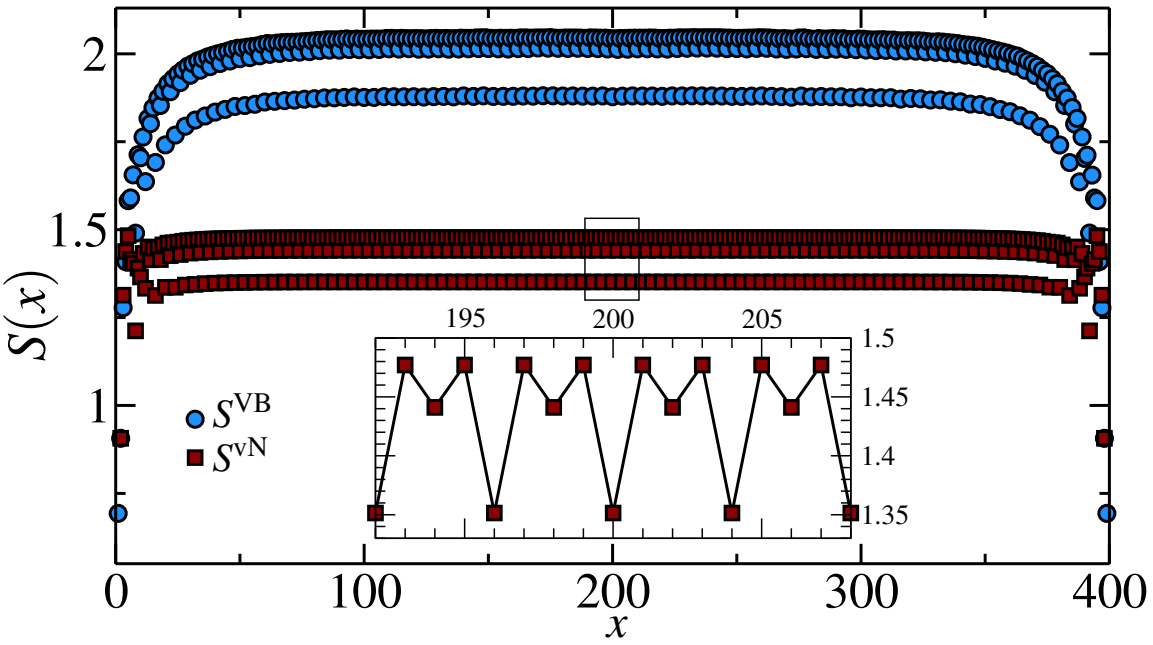

Figure 3.8: Entanglement entropies for a four-leg ladder with OBC and 100 sites per leg. The inset shows a close up view of the boxed region.

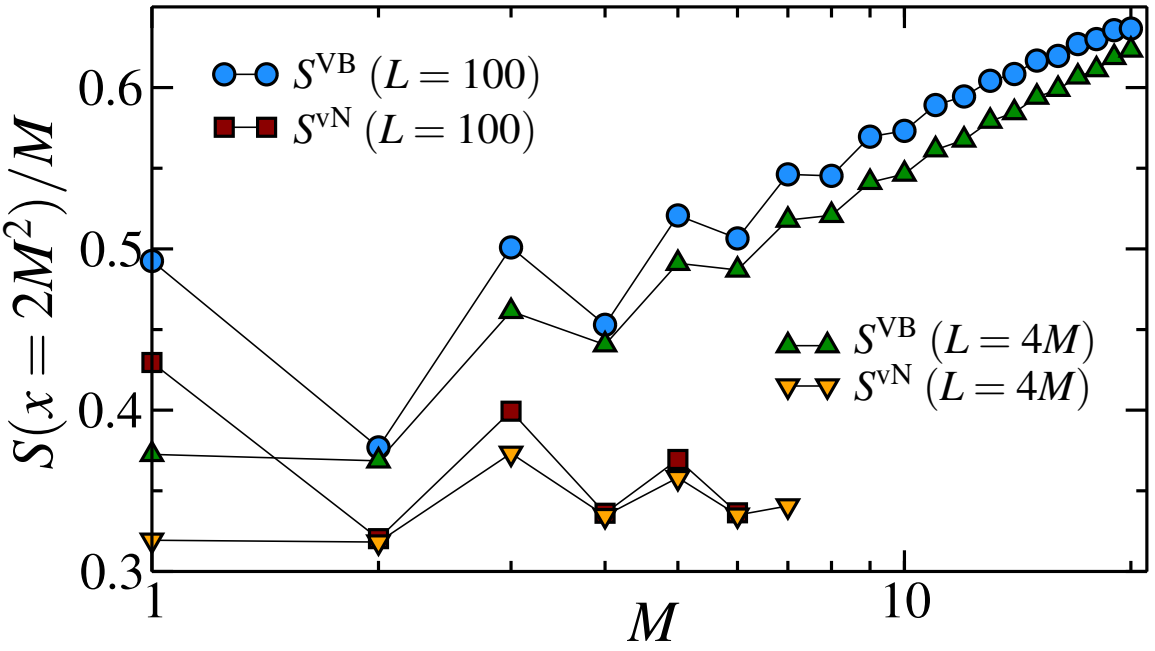

Figure 3.9: Entanglement entropies divided by M, for M-leg ladders, taken such that the region A includes $2M^2$ sites. Data from both ladders of with $L = 100$ sites per leg and ladders of length $L = 4M$ (with length proportional to the number of legs) are shown. For large M, $S^{\rm VB} \propto M \ln M$, whereas $S^{\rm vN} \propto M$.

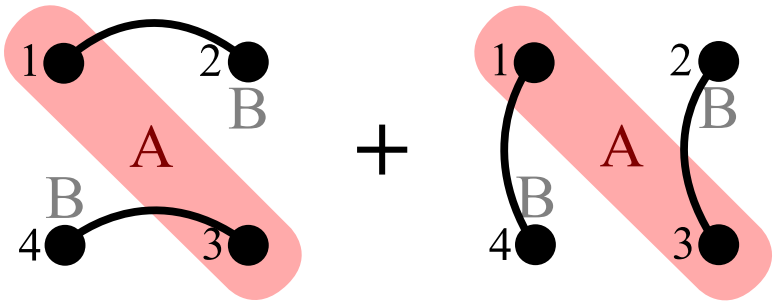

Figure 3.10: An equal superposition of two four-site valence bond states. Region A is the shaded region including sites 1 and 4. Region B contains sites 2 and 3. For this state $S_{\mathrm{A}}^{\mathrm{VB}} = 2\ln(2) \approx 1.386$ and $S_{\mathrm{A}}^{\mathrm{vN}} = \ln(3) \approx 1.099$.

We observe a multiplicative logarithmic correction to the area law in S^{VB}, as previously shown by Refs.[35, 36]. This correction, however, is not present in the S^{vN} results from DMRG. S^{vN} convincingly approaches a constant value for large M, suggesting that the area law is valid for S^{vN} in the $M \to \infty$ limit. These results also imply that the multiplicative logarithmic correction to the area law is present only in S^{VB}, and not necessarily in all measures of entanglement entropy.

3.4 Analytical Calculations

From the 1D results (Figs. 3.2 and 3.4) we saw that S^{VB} can be either greater or less than S^{vN}. This can be understood through some simple examples, shown in figures 3.10 and 3.11. The first example, Fig. 3.10 is an equal superposition of two four-site valence bond states. S^{VB} is easily calculated as the maximal value, $S^{\mathrm{VB}} = 2\ln(2)$, since there are four bonds crossing between regions A and B, and we divide by the number of states (two in this case). This corresponds to the way S^{VB} would be measured in the single projector VB QMC algorithm. For such a small system, it is not difficult to calculate S^{vN} explicitly, and we will do so here. We begin by writing out and normalizing the wavefunction in the S^z basis.

$$|\psi\rangle = C\big[\,(|\uparrow_1\downarrow_2\rangle - |\downarrow_1\uparrow_2\rangle) \otimes (|\uparrow_3\downarrow_4\rangle - |\downarrow_3\uparrow_4\rangle) + (|\uparrow_1\downarrow_4\rangle - |\downarrow_1\uparrow_4\rangle) \otimes (|\uparrow_3\downarrow_2\rangle - |\downarrow_3\uparrow_2\rangle)\,\big] \tag{3.4}$$

$$= C\big[2|\uparrow\downarrow\uparrow\downarrow\rangle + 2|\downarrow\uparrow\downarrow\uparrow\rangle - |\uparrow\downarrow\downarrow\uparrow\rangle - |\downarrow\uparrow\uparrow\downarrow\rangle - |\uparrow\uparrow\downarrow\downarrow\rangle - |\downarrow\downarrow\uparrow\uparrow\rangle\big] \tag{3.5}$$

$$C = \frac{1}{\sqrt{\langle\psi|\psi\rangle}} = \frac{1}{\sqrt{4+4+1+1+1+1}} = \frac{1}{\sqrt{12}} \tag{3.6}$$

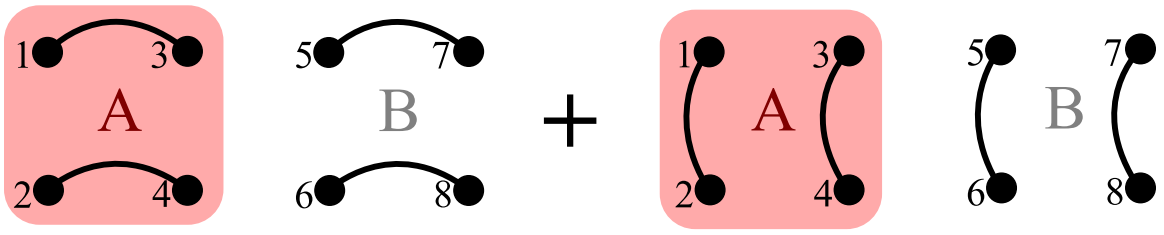

Figure 3.11: An equal superposition of two eight-site states. Region A is the shaded region including sites $1-4$. Region B contains the remainder of the sites, $5-8$. For this state $S_{\rm A}^{\rm VB}=0$ and $S_{\rm A}^{\rm vN}\approx 0.325$.

Note that in (3.5) the spins are in numerical order $|1,2,3,4\rangle$. To simplify the process of finding the reduced density matrix $\rho_{\rm A}$ we relabel the states such that

$$|\uparrow\uparrow\rangle\rightarrow|a\rangle \qquad |\uparrow\downarrow\rangle\rightarrow|b\rangle \qquad |\downarrow\uparrow\rangle\rightarrow|c\rangle \qquad |\downarrow\downarrow\rangle\rightarrow|d\rangle, \tag{3.7}$$

and a subscript A specifies that the state belongs to spins 1 and 3, while B refers to spins 2 and 4.

$$|\psi\rangle=\frac{1}{\sqrt{12}}\big[2|a\rangle_{\rm A}\otimes|d\rangle_{\rm B}+2|d\rangle_{\rm A}\otimes|a\rangle_{\rm B}-\big(|b\rangle+|c\rangle\big)_{\rm A}\otimes|c\rangle_{\rm B}-\big(|c\rangle+|b\rangle\big)_{\rm A}\otimes|b\rangle_{\rm B}\big] \tag{3.8}$$

When we trace out region B, only the terms that are diagonal in region B will survive. We can avoid writing out the full density matrix and skip straight to the reduced density matrix. Now all the states refer to region A, spins 1 and 3.

$$\rho_{\rm A}={\rm Tr}_{\rm B}|\psi\rangle\langle\psi| \tag{3.9}$$

$$=\frac{1}{12}\big[4|a\rangle\langle a|+4|d\rangle\langle d|+2\big(|b\rangle+|c\rangle\big)\big(\langle b|+\langle c|\big)\big]=\frac{1}{6}\begin{bmatrix}2&0&0&0\\0&1&1&0\\0&1&1&0\\0&0&0&2\end{bmatrix} \tag{3.10}$$

Diagonalizing $\rho_{\rm A}$ gives three non-zero eigenvalues all equal to $\frac{1}{3}$, which we use to calculate $S^{\rm vN}$,

$$S_{\rm A}^{\rm vN}=-{\rm Tr}\left(\rho_{\rm A}\ln\rho_{\rm A}\right)=-3\left(\frac{1}{3}\ln\left(\frac{1}{3}\right)\right)=\ln(3)\approx 1.0986. \tag{3.11}$$

For this system (Fig. 3.10) $S^{\rm VB}=2\ln(2)>S^{\rm vN}\approx 1.0986$. Though $S^{\rm VB}=S^{\rm vN}$ for non-superpositional valence bond basis states, $S^{\rm VB}$ does not give the correct result for some linear combinations of such states.

In Figure 3.11 we have another linear combination of states, this time a superposition of two eight-site states, where region A includes the four sites on the left-hand side. In

this case we find that $S^{\rm VB}$ underestimates $S^{\rm vN}$ since there are no valence bonds crossing between regions A and B, but the two regions are still entangled. The calculation of $S^{\rm vN}$ for this state can be seen in Appendix B, where we find $S^{\rm vN} \approx 0.3251$.

3.5 Discussion

We have compared the scaling properties of the valence bond entanglement entropy $S^{\rm VB}$ [35, 36], to the von Neumann entanglement entropy $S^{\rm vN}$ in the spin-1/2 Heisenberg model in 1D and on multi-leg ladder systems, using both VB QMC and DMRG simulations methods. In 1D, we find that $S^{\rm VB}$ closely follows the behavior of $S^{\rm vN}$, though it is less than $S^{\rm vN}$ for periodic chains, and greater than $S^{\rm vN}$ for chains with open boundaries.

We also fit both entanglement entropies to the 1D conformal field theory results (Eqs.(3.2) and (3.3)), which show excellent agreement for $S^{\rm vN}$, but show significant deviation from the expected value of c for $S^{\rm VB}$ in the large chain length limit, approaching $c < 1$ for both open and periodic boundary conditions [42].

We then examined M-leg ladder systems, cutting across all legs such that the boundary size scales with the number of legs, where we see from the DMRG results that $S^{\rm vN}$ obeys the area law in the many-leg limit. On the other hand, $S^{\rm VB}$ has a multiplicative logarithmic correction to the area law for the Néel ground state. This correction may be due to the fact that the valence bond basis is massively overcomplete. In general, for some valence bond basis states ψ_1 and ψ_2, $S^{\rm vN}(\psi_1+\psi_2) \neq S^{\rm vN}(\psi_1)+S^{\rm vN}(\psi_2)$, however we use $S^{\rm VB}(\psi_1+\psi_2) = S^{\rm VB}(\psi_1)+S^{\rm VB}(\psi_2)$ to get the valence bond entanglement entropy

The $S^{\rm VB}$ is a reasonable measure of entanglement, that is easily accessible to scalable numerical simulations. Our demonstration that $S^{\rm VB}$ is unable to give a bound on $S^{\rm vN}$, an in particular its multiplicative log correction to the area law in 2D, make it unsuitable to characterize e.g. topologcal phases using measurements based on additive subleading corrections to area law scaling in vN, such as the topological entanglement entropy.

In the next chapter we explore an alternative method for measuring entanglement in large-scale quantum Monte Carlo simulations.

Chapter 4

Measuring Renyi Entanglement Entropy

Though we are not able to measure S^{vN} in VB QMC simulations, due to the inaccessiblity of the wavefunction of the system, using a "replica trick" we are able to measure $\text{Tr}(\rho_{\text{A}}^n)$ in our algorithm for $n > 1$, which allows us to measure the Renyi entanglement entropies

$$S_n(\rho_{\text{A}}) = \frac{1}{1-n} \ln \left[\text{Tr} \left(\rho_{\text{A}}^n \right) \right], \tag{4.1}$$

for $n > 1$. For $n > m$ these entropies have the property that $S_n \leq S_m$, so the second Renyi entropy, S_2 will give the largest lower bound on S^{vN}. The Renyi entropies are expected to follow the same area laws obeyed by S^{vN} [11], making them equally useful in the study of universal quantities. The Renyi entropies together also encode information about the whole entanglement spectrum of the system, and thus contain more information that S^{vN} alone [11].

In this chapter we begin by demonstrating the measurement of $\text{Tr}(\rho_{\text{A}}^n)$ using a replica trick, and we show the specific case for $n = 2$ using a *Swap* operator on two copies of a system. We measure S_2 in 1D first, using a double projector VB QMC algorithm and comparing the results to DMRG results for S_2. We also show results generated using the loop algorithm. We develop a method to improve the sampling of our S_2 measurement using a different Monte Carlo weight, and measuring the ratio of $Swap_{\text{A}}$ operators for different sizes of region A. We then move to 2D, approaching the limit of DMRG simulations, and look at both $L \times L$ systems with periodic boundary conditions, and M-leg ladders, as in the previous chapter, with open boundary conditions. We find area law scaling of the entanglement entropy in both of these geometries [44].

For this project I measured S_2 with the bare $Swap_{\text{A}}$ operator using both a double projector VB QMC program, and a loop algorithm VB QMC program. I also measured

a ratio of $Swap_{\mathrm{A}}$ operators using a double projector code. DMRG measurements were performed by I. González and R. Melko.

4.1 The "Replica Trick"

In order to calculate $\mathrm{Tr}(\rho_{\mathrm{A}}^n)$, a quantity necessary to measure the n^{th} Renyi entanglement entropy for $n \geq 2$, we use a trick involving replicas of the system to be studied, Ψ_0. We simulate n non-interacting replicas of the system. The expectation value of a swap operator is measured. The purpose of the swap operator is to swap the state of the system in region A between the non-interacting replicas. Calculating the expectation value of this operator accomplishes two things: it (1) reorganizes the replicas $\langle \Psi_0 \otimes \Psi_0 \otimes \cdots \otimes \Psi_0 |$ and $|\Psi_0 \otimes \Psi_0 \otimes \cdots \otimes \Psi_0\rangle$ into the density matrix ρ^n while simultaneously (2) tracing out region B of the system. This process is independent of the basis used, as the swap operator can be defined in any basis. We using this method in the valence bond basis, but it has since been employed in finite temperature stochastic series expansion quantum Monte Carlo [45], which uses the S^z basis. Below we show a method using two non-interacting copies of a system, and a $Swap_{\mathrm{A}}$ operator, to measure $\mathrm{Tr}(\rho_{\mathrm{A}}^2)$, which is necessary for the calculation of S_2 .

4.1.1 The Swap Operator

The $Swap_{\mathrm{A}}$ operator acts on two copies of the system (see Figure 4.1), where the copies are not necessarily in the same state. The action of $Swap_{\mathrm{A}}$ is to exchange the configuration of region A, between the two copies of the system. If region A has some entanglement with region B in one or both of the copies of the system, then the two copies will become entangled after the application of $Swap_{\mathrm{A}}$. The $Swap_{\mathrm{A}}$ operator can be more clearly defined in a product basis such as the S^z basis, in which an arbitrary state can be represented as a weighted sum of states decomposed into the separate a region A and a region B configuration. If we define $\{|\alpha\rangle\}$ as a complete basis of states spanning region A, and $\{|\beta\rangle\}$ as a complete basis of states spanning region B, then we can represent an arbitrary state as

$$|\psi\rangle = \sum_{\alpha} \sum_{\beta} C_{\alpha,\beta} |\alpha\rangle |\beta\rangle \tag{4.2}$$

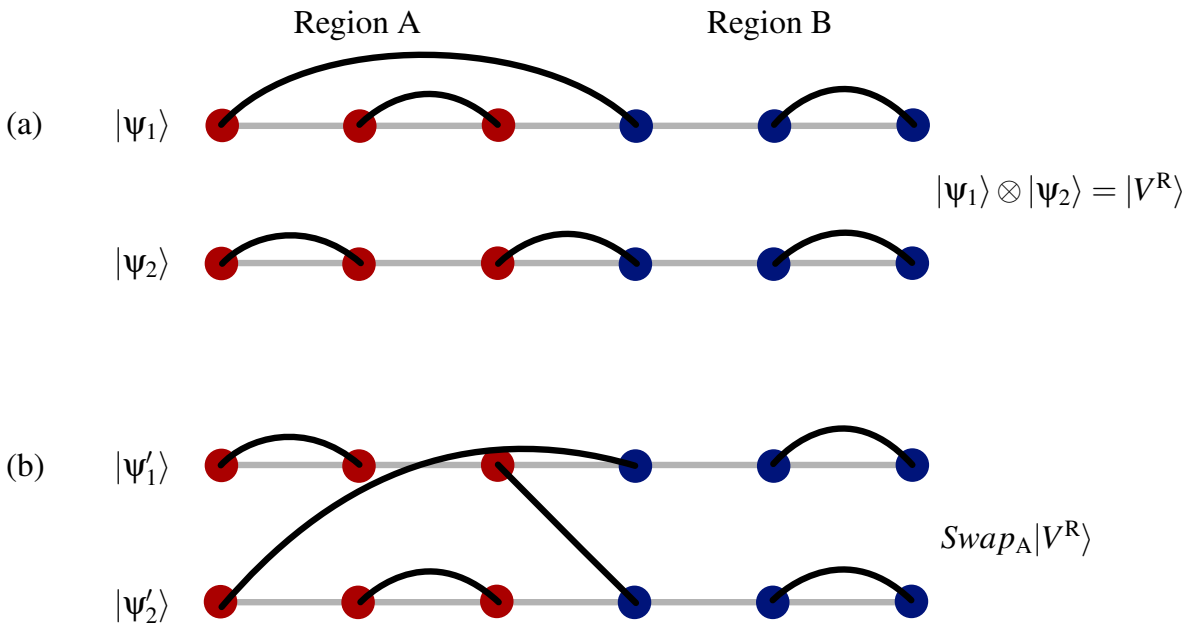

Figure 4.1: (a) Two non-interacting copies, $|\psi_1\rangle$ and $|\psi_2\rangle$, of a six-site chain where the left three sites of each copy belong to region A, and the other sites are in region B.
(b) The same system from (a) after the $Swap_{\mathrm{A}}$ operator is applied. The endpoints of the valence bonds in region A are swapped between copies of the system. Region B remains unswapped.

for some set of coefficients $C_{\alpha,\beta}$. Then the effect of $Swap_{\mathrm{A}}$ on a two general states, $|\psi_1\rangle$ and $|\psi_2\rangle$ representing the two copies of the system, is

$$Swap_{\mathrm{A}}|\psi_1\rangle \otimes |\psi_2\rangle = Swap_{\mathrm{A}} \left(\sum_{\alpha_1,\beta_1} C_{\alpha_1,\beta_1} |\alpha_1\rangle|\beta_1\rangle \right) \otimes \left(\sum_{\alpha_2,\beta_2} C_{\alpha_2,\beta_2} |\alpha_2\rangle|\beta_2\rangle \right) \tag{4.3}$$

$$= \sum_{\alpha_1,\beta_1} C_{\alpha_1,\beta_1} \sum_{\alpha_2,\beta_2} C_{\alpha_2,\beta_2} \big(|\alpha_2\rangle|\beta_1\rangle\big) \otimes \big(|\alpha_1\rangle|\beta_2\rangle\big). \tag{4.4}$$

And the expectation value of $Swap_{\mathrm{A}}$ acting on two non-interacting copies of the ground state will be

$$\langle Swap_{\mathrm{A}} \rangle = \langle \Psi_0 \otimes \Psi_0 | Swap_{\mathrm{A}} | \Psi_0 \otimes \Psi_0 \rangle \tag{4.5}$$

$$= \sum_{\alpha_1,\beta_1} \sum_{\alpha_2,\beta_2} \overline{C}_{\alpha_2,\beta_1} C_{\alpha_1,\beta_1} \overline{C}_{\alpha_1,\beta_2} C_{\alpha_2,\beta_2} \tag{4.6}$$

$$= \sum_{\alpha_1,\alpha_2} \langle \alpha_1 | \rho_{\mathrm{A}} | \alpha_2 \rangle \langle \alpha_2 | \rho_{\mathrm{A}} | \alpha_1 \rangle \tag{4.7}$$

$$= \mathrm{Tr}(\rho_{\mathrm{A}}^2). \tag{4.8}$$

For more detail see Appendix A. From Equation (1.6) the second Renyi entanglement entropy is

$$S_2(\rho_{\mathrm{A}}) = -\ln\big[\mathrm{Tr}(\rho_{\mathrm{A}}^2)\big] = -\ln\left(\langle Swap_{\mathrm{A}} \rangle\right), \tag{4.9}$$

independent of basis. Specifically, we can use (4.9) in the valence bond basis, where the $Swap_{\mathrm{A}}$ operator acts to swap the endpoints of valence bonds within region A between copies of the system, as in Figure 4.1.

4.1.2 Measuring the Swap Operator

Since we are using the double projector algorithm for these measurements (Section 2.4.2) we use equations (2.45) and (2.46) to measure the $Swap_{\mathrm{A}}$ operator,

$$\langle Swap_{\mathrm{A}} \rangle = \frac{\sum_{l,r} W_l^L W_r^R \langle V_l^L | V_r^R \rangle \frac{\langle V_l^L | Swap_{\mathrm{A}} | V_r^R \rangle}{\langle V_l^L | V_r^R \rangle}}{\sum_{l,r} W_l^L W_r^R \langle V_l^L | V_r^R \rangle} = \left\langle \frac{\langle V^L | Swap_{\mathrm{A}} | V^R \rangle}{\langle V^L | V^R \rangle} \right\rangle, \tag{4.10}$$

though in this case $|V^{\mathrm{L}}\rangle$ and $|V^{\mathrm{R}}\rangle$ each contain two non-interacting copies of the system we want to study, depicted in Fig. 4.1.

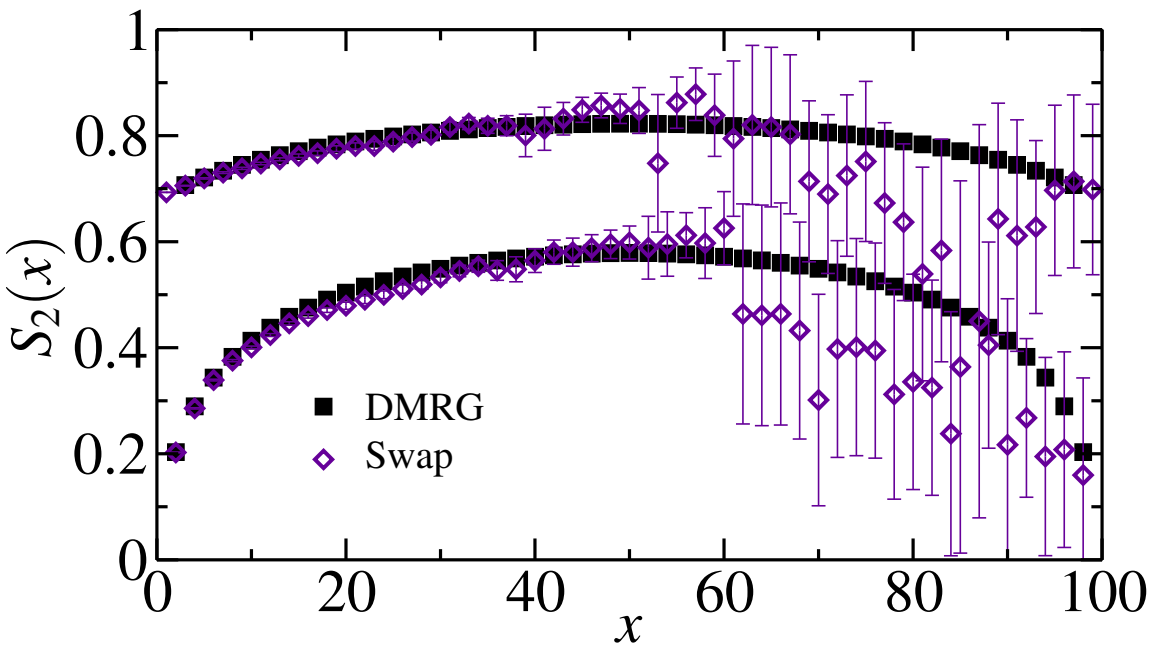

Figure 4.2: The Renyi entropy S_2 as a function of site index $x \in$ A, for a 100-site Heisenberg chain with open boundaries, calculated with DMRG and VB QMC. Data labeled "Swap" was calculated with Eq. (4.10) with one VB QMC simulation.

4.2 1D Results

We begin by measuring S_2 for a 1D OBC chain of length $L = 100$, using the expectation value of the $Swap_x$ operator to find S_2 in VB QMC, where sites 1 through x are included in region A. The trial state $|V\rangle$ used is a simple dimerized state with only nearest neighbor valence bonds. Results are shown in Figure 4.2. In the DMRG simulations, S_2 is calculated in the standard way, using the eigenvalues of the reduced density matrix. One can immediately see that the calculation of S_2 with the expectation value $\langle Swap_{\mathrm{A}}\rangle$ gives very large statistical errors, especially for a large number of sites inside region A.

One way to understand this result is to consider what we are actually measuring. From Eq. (4.10) one can see we are measuring the ratio of two inner products. Since the overlap (Eq. (2.24)) is $2^{N_{\mathrm{loop}}-N_{\mathrm{sites}}/2}$, this ratio of inner products is $2^{N_{\mathrm{swaploops}}-N_{\mathrm{loops}}}$. The quantity we measure depends entirely on the change in the number of loops after applying a swap operator to one of our states. For a large region A we are swapping a larger number of sites, and the difference in the number of loops can change by a large range of values. We have to sample states for much longer to converge on the average change in the number of loops. In contrast, swapping only one site ($x = 1$) will always decrease the number of loops by 1, so $S_2(1) = \ln(2)$ always. For two sites in region A, the difference in the number of loops can be -2 or 0. So for a small region A, the change in the number of loops has fewer possible values.

One way to improve upon the poor sampling of $\langle Swap_{\mathrm{A}}\rangle$ is using the loop algorithm (Section 2.4.3), which scales as m while the double projector method scales like Nm. Measurements taken using the loop algorithm are added in Figure 4.3; they show a significant improvement over the double projector $\langle Swap_{\mathrm{A}}\rangle$ measurement, though there is still noticeable statistical error for large region A. If our goal was simply the measurement of S_2 instead of the demonstration of the most effective way to measure S_2, we could note that $S_2(A) = S_2(B)$ and reflect the data about the midpoint, resulting in almost perfect correspondence with the DMRG data. However, when we begin to measure larger system sizes and move to 2D the deficiencies in measuring the bare $Swap_{\mathrm{A}}$ operator will become increasingly apparent; it is necessary to improve upon this measurement technique, which we have done using an "improved ratio" sampling scheme.

4.3 "Improved Ratio" Sampling

Instead of measuring $\langle Swap_x\rangle$ for a region A including x sites, we measure a ratio of different $Swap_x$ operators,

$$\frac{\langle Swap_{x+j}\rangle}{\langle Swap_x\rangle} = \frac{\sum_{i,k} W_i^L W_k^R \langle V_i^L|Swap_{x+j}|V_k^R\rangle}{\sum_{i,k} W_i^L W_k^R \langle V_i^L|Swap_x|V_k^R\rangle}, \tag{4.11}$$

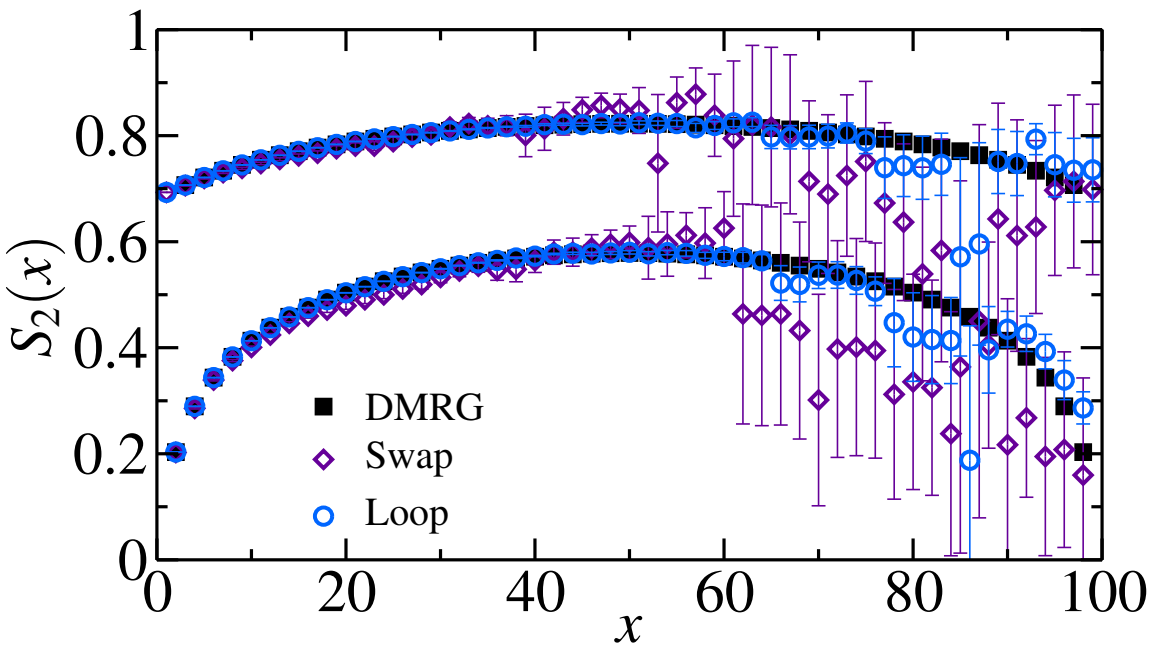

Figure 4.3: The Renyi entropy S_2 as a function of site index $x \in$ A, for a 100-site Heisenberg chain with open boundaries, calculated with DMRG, VB QMC double projector algorithm (labelled Swap), and the VB QMC loop algorithm (labelled Loop).

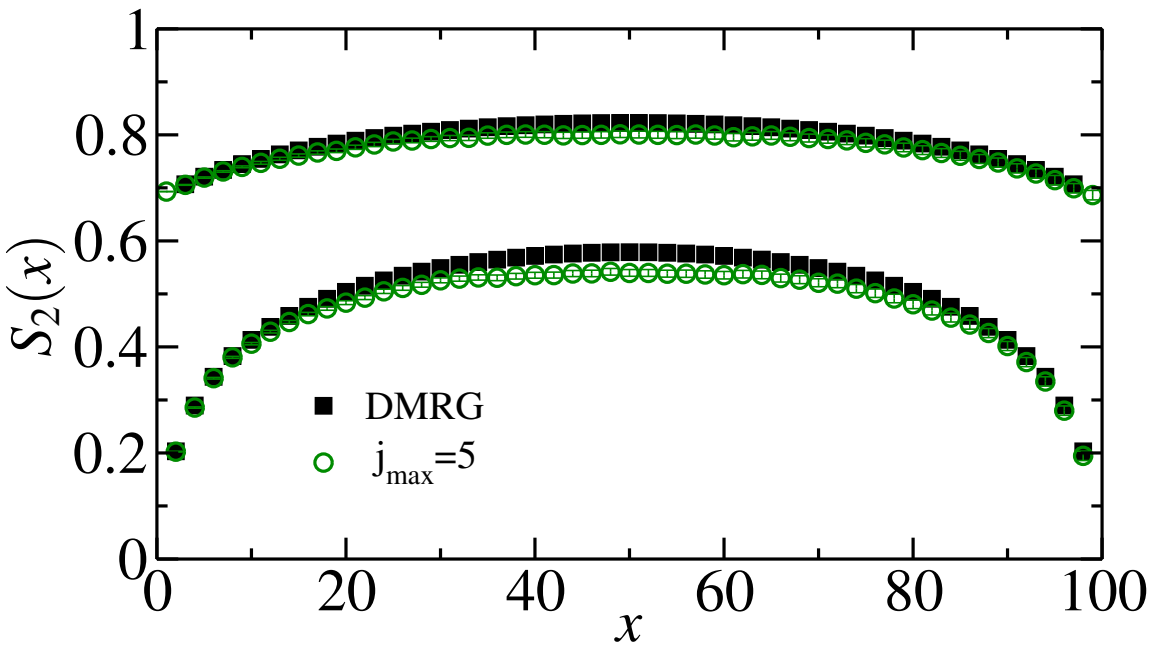

Figure 4.4: DMRG and improved ratio data for a 100-site Heisenberg chain with open boundaries. The ratio data uses $j_{\max} = 5$ and requires 20 separate simulations.

where $j = 1, \ldots, j_{\max}$ is the difference between the region sizes for the two $Swap$ operators. To get to the entanglement entropy from here we take the negative logarithm of (4.11) to get

$$-\ln\left(\frac{\langle Swap_{x+j}\rangle}{\langle Swap_x\rangle}\right) = -\ln\langle Swap_{x+j}\rangle + \ln\langle Swap_x\rangle = S_2(x+j) - S_2(x), \tag{4.12}$$

so we can extract $S_2(x+j)$ if we have $S_2(x)$ from a previous measurement. The sampling weight from (2.44) is modified with this new measurement, to be

$$W_{\text{total}} = W^L W^R \langle V^L | Swap_x | V^R \rangle. \tag{4.13}$$

However, modifying the sampling weight in this way means we can only measure the ratio (4.11) for one value of x per simulation. To get S_2 for all region sizes we first choose a value for $j_{\max}$. A small $j_{\max}$ means more improvement due to the ratio, but also more simulations are required. We then measure the bare $\langle Swap_j\rangle$ for $j = 1, \ldots, j_{\max}$ in our first simulation. The second simulation measures the ratio $\langle Swap_{x+j}\rangle/\langle Swap_x\rangle$ with $x = j_{\max}$. The following simulations use $x = 2j_{\max}, 3j_{\max}, 4j_{\max}, \ldots$ until we reach the maximum size of region A. The number of simulations need for a 1D system is $(L/j_{\max})$.

Figure 4.4 shows the ratio data using $j_{\max} = 5$, along with the DMRG data, for the same 100-site system as in Figs. 4.3 and 4.2. The data no longer show the large statistical

error bars for large region A sizes, though the results are systematically lower than the DMRG S_2 results for a region A-B boundary near the middle of the 100-site system. The improved ratio sampling unfortunately introduces a new source of systematic error not accounted for by our error bars. S_2 measurements for larger region sizes depend on the previous measurements, thus if a measurement for a small region A has some error, that will carry through to all other measurements, as one can see when comparing the regions of size $x = 1$ and $x = 99$ in Figure 4.4.

4.4 2D Results

We now look at 2D $L \times L$ systems with PBC, where region A is an $\ell \times \ell$ and region B is the remainder of the system. For this system we must slightly change the definition of our improved ratio estimator to fit the different geometry. Instead of j and $j_{\max}$ from (4.11) and (4.12) we now use r and $r_{\max}$, and measure $\langle Swap_{\ell+r}\rangle / \langle Swap_{\ell}\rangle$ where $\ell + r$ is the linear dimension of a square region A, and $r = 1, \ldots, r_{\max}$. We increase the size of region A such that it is always a square, adding a row and column of sites simultaneously.

Figure 4.5 shows the *Swap* and ratio results for 2D PBC systems of size 8×8 and 12×12. For the 8×8 system the results are already almost entirely converged with the *Swap* measurement, and the ratio measurements only offer a very slight improvement. When the system size is increased to 12×12 the ratio results significantly improve the measurement, though the $r_{\max} = 2$ and $r_{\max} = 1$ results almost exactly overlap, implying that the results have converged to the correct answer at that point. It is possible to improve the sampling even further adding one site at a time to the region size, instead of only increasing the linear dimension of region A. We should note that for large values of $r_{\max}$ the correct value of S_2 does not fall within the error bars of the data, indicating that the low sampling of the *Swap* operator may weaken the ergodicity of the simulation.

4.5 The Area Law

Using the improved ratio estimator we now examine larger systems of the same geometry as was used in the previous section (PBC $L \times L$ systems with an $\ell \times \ell$ region A) in an attempt to extract area law scaling of the entanglement entropy. Figure 4.6 show S_2/ℓ results for systems from $L = 4$ to $L = 32$. From Section 3.3 and Ref. [38] one expects the scaling of $S_1 = S^{\mathrm{vN}}$ in the Néel state to follow the area law, and we know that $S_2 \leq S^{\mathrm{vN}}$. The data in Fig. 4.6 appears consistent with the area law $S_2/\ell \sim$ const. for $\ell \ll L$, in particular we do not see a multiplicative log correction that was present in the scaling of S^{VB} [35, 36].

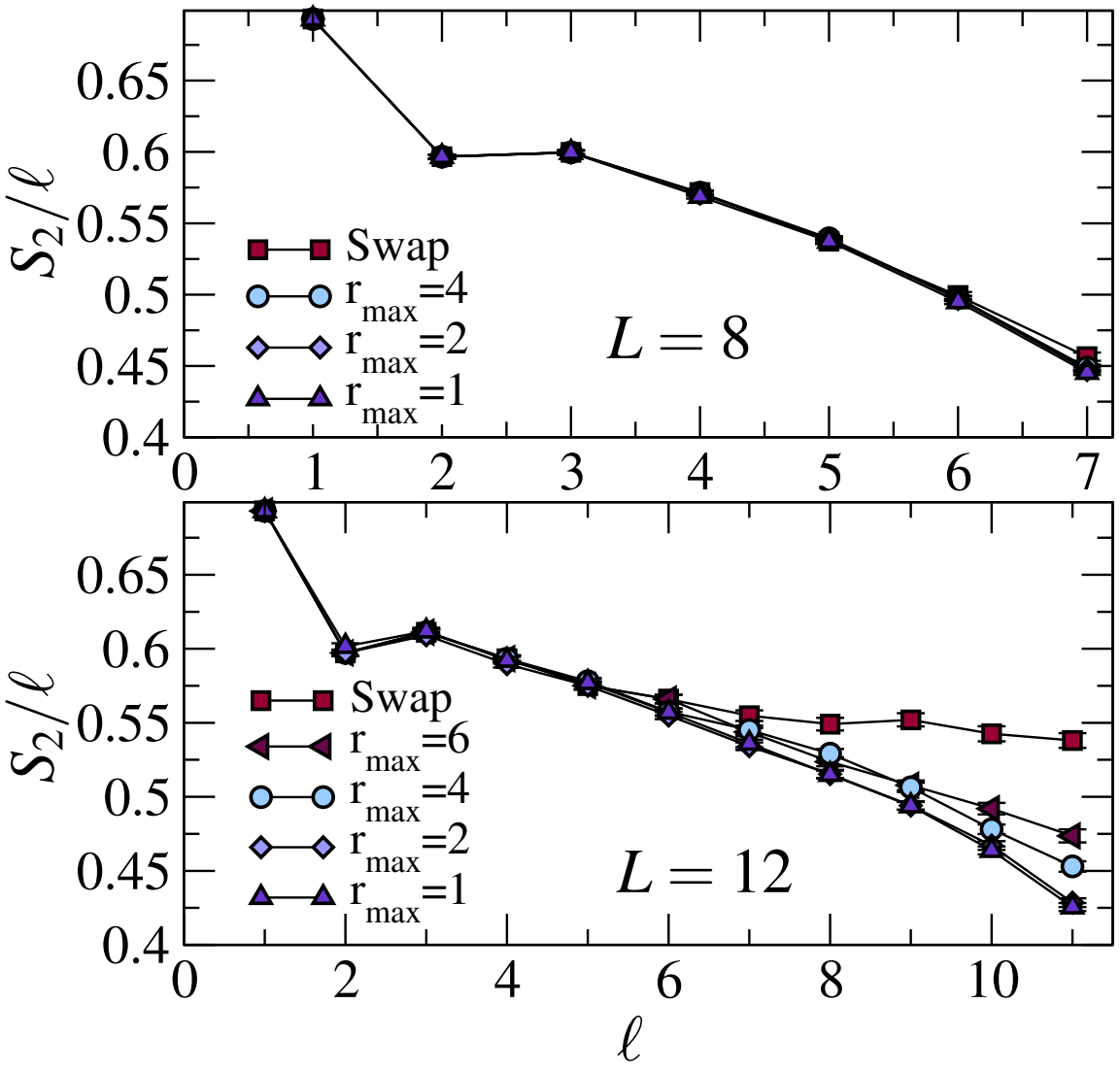

Figure 4.5: Measurements of S_2/ℓ for 8×8 and 12×12 PBC systems with a region A of size ℓ. The bare $\langle Swap_\ell \rangle$ results are shown along with the improved ratio results for different values of $r_{\max}$.

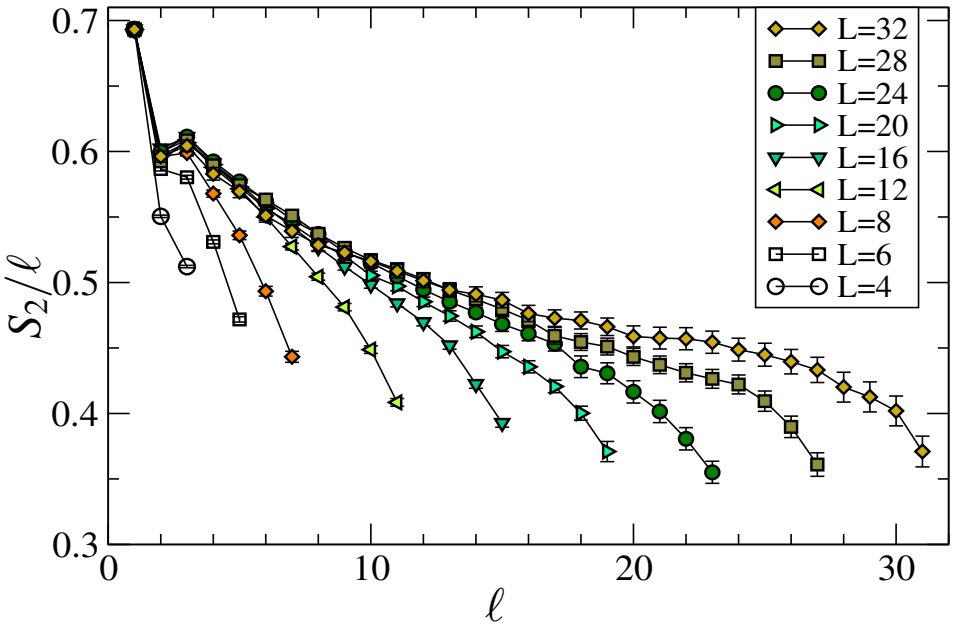

Figure 4.6: Scaling of the entanglement entropy S_2/ℓ plotted versus ℓ for different sizes of the $\ell \times \ell$ region A and different $L \times L$ system sizes. The data are calculated using the 2D improved ratio estimator (4.11) with $r_{\max} = 1$.

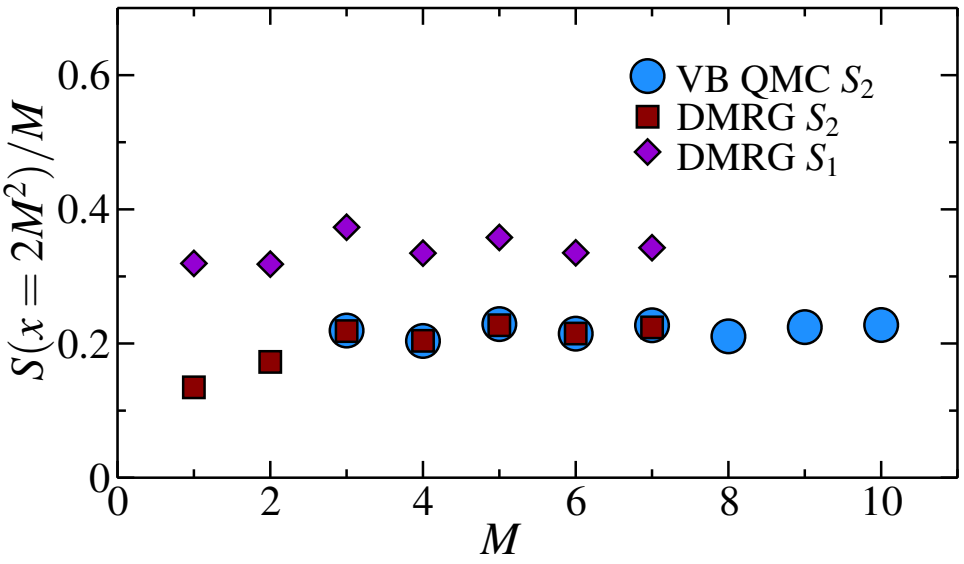

Figure 4.7: Scaling of the von Neumann and second Renui entanglement entropies S/M plotted versus M, for M-leg ladders of length $4M$. Region A contains $2M^2$ sites, dividing the ladders in half with the cut is across the M legs, using one of the same geometries as is found in Fig. 3.9. The data were measured using the 2D improved ratio estimator using $j_{\max} = M$.

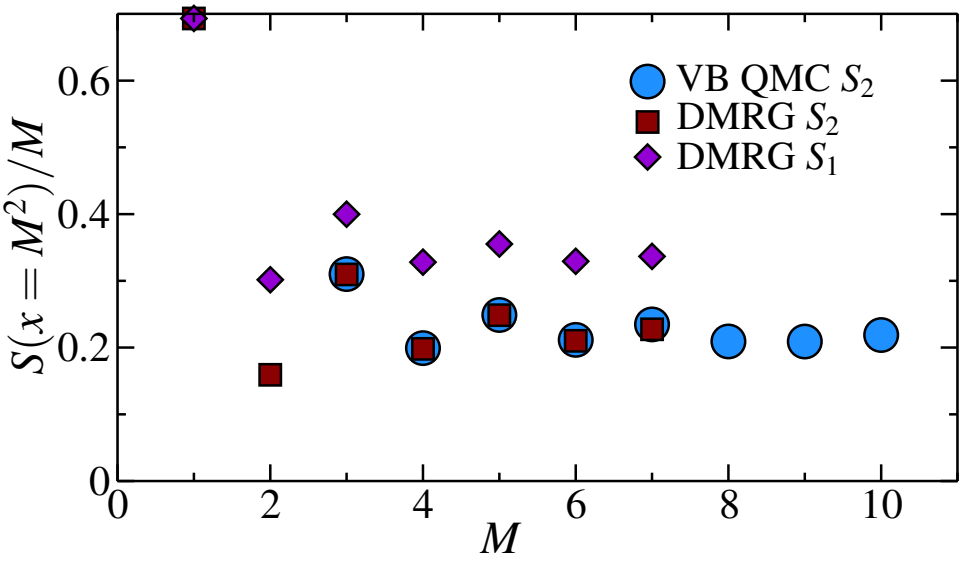

Figure 4.8: Scaling of the von Neumann and second Renyi entanglement entropies S/M plotted versus M, for M-leg ladders of length $4M$. Region A contains M^2 sites, dividing the ladders into segments one-quarter and three-quarters of its length, where the cut is across the M legs. This geometry is quite similar to one of the geometries used in Fig 3.9. The data were measured using the 2D improved ratio estimator using $j_{\max} = M$.

Next we examine entanglement entropy scaling for the ladder geometry studied in Section 3.3 and Ref. [38]. The results are shown in Figure 4.7, including both DMRG and ratio estimator VB QMC data. From the DMRG data alone it is not immediately apparent that $S_2/M \sim$ const., especially considering the trend in the first few data points. Fortunately, the range of system sizes we can study is extended by the $Swap_{\mathrm{A}}$ measurement with VB QMC, and the added points make it clear that S_2 does in fact follow an area law for the Néel state.

In Figure 4.8 we examine the same systems with only M^2 sites in region A. For the small system sizes we see much larger even-odd oscillations, as we go to larger system sizes both Figs. 4.7 and 4.8 follow the same area law scaling.

4.6 Discussion

We have presented a method which can be used to measure the Renyi entropies for $n > 1$, with quantum Monte Carlo simulations in the valence bond basis, employing a "replica trick". We demonstrate this method by measuring the second Renyi entropy S_2 using the expectation value of a $Swap_{\mathrm{A}}$ operator acting on two copies of the system. With the use of a ratio estimator we improve the sampling of our algorithm and our results for S_2 converge to the exact results for a 1D Heisenberg chain with open boundaries. Using this same method we present the first measurements of S_2 on 2D periodic $L \times L$ and open boundary ladder systems, confirming the area law for the Néel ground state of the Heisenberg model.

Chapter 5

Conclusions

In this thesis we have examined methods for measuring entanglement entropy in spin-1/2 Heisenberg systems using quantum Monte Carlo in the valence bond basis. We began by presenting the quantum Monte Carlo techniques used in this research: the single projector method, the double projector method, and the loop algorithm.

We then used the single projector method technique to directly compare the recently proposed valence bond entanglement entropy to the standard definition of entanglement entropy: the von Neumann entanglement entropy, measured using density matrix renormalization group simulations. We found that the valence bond entanglement entropy, unlike the Renyi entanglement entropies, does not give a bound on the von Neumann entanglement entropy, and that it exhibits a multiplicative logarithmic correction to the area law scaling, which is not present in the scaling of the von Neumann entanglement entropy. Though the valence bond entanglement entropy has the advantage of its simplicity of measurement, presence of the multiplicative correction to the area law scaling may make it unsuitable to study universal additive subleading corrections to area law scaling in vN.

We then presented a method to measure the generalized Renyi entanglement entropies (excluding S_1) through the expectation value of a $Swap$ operator acting on non-interacting copies of a system. Measurements of the second Renyi entropy were done using double projector valence bond quantum Monte Carlo and results were compared to those obtained using density matrix renormalization group simulations. We found the Monte Carlo results converged to the exact DMRG results for one dimensional Heisenberg spin-1/2 chains. We also saw, using both an M leg ladder geometry and a torus geometry, that the scaling of the second Renyi entropy follows an area law in the two dimensional Heisenberg ground state.

In the future we hope to improve the sampling of our Renyi measurement to the point where it is possible to extract subleading corrections to the area law. One way we may

accomplish this is by experimenting with different reweighting schemes for the measurement of the *Swap* operator. There is a technique called *multicanonical sampling* [46, 47] which allows the simulation to reach every point in the space of values of $\langle Swap \rangle$ with equal probability with the help of a weighting function.

The measurement of Renyi entropy has already been extended to use in finite temperature Stochastic Series Expansion quantum Monte Carlo simulations [45], where it was found that the mutual information (a quantity related to the difference on Renyi entropies) converges to a limiting function of temperature, with apparently nontrivial corrections near critical points. Further measurements in systems near critical points could allow the extraction of a suspected universal critical exponent present in the scaling of mutual information.

We have developed the first method that can be used to measure entanglement entropy in condensed matter systems with a scalable simulation technique. This will allow us to use quantum Monte Carlo simulations of entanglement entropy to characterize novel quantum phases and phase trasitions, including measuring new universal quantities at critical points, through the subleading corrections to the area law.

APPENDICES

Appendix A

Expectation Value of the Swap Operator

$$\langle Swap_{\mathrm{A}} \rangle = \langle \Psi_0 \otimes \Psi_0 | Swap_{\mathrm{A}} | \Psi_0 \otimes \Psi_0 \rangle \tag{A.1}$$

$$= \left(\sum_{\alpha_1', \beta_1'} \overline{C}_{\alpha_1', \beta_1'} \sum_{\alpha_2', \beta_2'} \overline{C}_{\alpha_2', \beta_2'} \big(\langle \alpha_1' | \langle \beta_1' | \big) \otimes \big(\langle \alpha_2' | \langle \beta_2' | \big) \right) \times$$

$$\left(\sum_{\alpha_1, \beta_1} C_{\alpha_1, \beta_1} \sum_{\alpha_2, \beta_2} C_{\alpha_2, \beta_2} \big(|\alpha_2\rangle | \beta_1 \rangle \big) \otimes \big(|\alpha_1\rangle | \beta_2 \rangle \big) \right) \tag{A.2}$$

$$= \sum_{\alpha_1', \beta_1'} \sum_{\alpha_1, \beta_1} \overline{C}_{\alpha_1', \beta_1'} C_{\alpha_1, \beta_1} \sum_{\alpha_2', \beta_2'} \sum_{\alpha_2, \beta_2} \overline{C}_{\alpha_2', \beta_2'} C_{\alpha_2, \beta_2} \langle \alpha_1' | \alpha_2 \rangle \langle \beta_1' | \beta_1 \rangle \langle \alpha_2' | \alpha_1 \rangle \langle \beta_2' | \beta_2 \rangle \tag{A.3}$$

$$= \sum_{\alpha_1, \beta_1} \sum_{\alpha_2, \beta_2} \overline{C}_{\alpha_2, \beta_1} C_{\alpha_1, \beta_1} \overline{C}_{\alpha_1, \beta_2} C_{\alpha_2, \beta_2} \tag{A.4}$$

$$= \sum_{\alpha_1, \alpha_2} \left(\sum_{\beta_1} C_{\alpha_1, \beta_1} \overline{C}_{\alpha_2, \beta_1} \right) \left(\sum_{\beta_2} C_{\alpha_2, \beta_2} \overline{C}_{\alpha_1, \beta_2} \right) \tag{A.5}$$

We should pause here to work backwards for a bit.

$$\rho_{\mathrm{A}} = \mathrm{Tr}_{\mathrm{B}}|\Psi_0\rangle\langle\Psi_0| \tag{A.6}$$

$$= \mathrm{Tr}_{\mathrm{B}}\left[\left(\sum_{\alpha_1,\beta_1} C_{\alpha_1,\beta_1}|\alpha_1\rangle|\beta_1\rangle\right)\left(\sum_{\alpha_2,\beta_2} \overline{C}_{\alpha_2,\beta_2}\langle\alpha_2|\langle\beta_2|\right)\right] \tag{A.7}$$

$$= \sum_{\beta_3}\langle\beta_3|\left[\left(\sum_{\alpha_1,\beta_1} C_{\alpha_1,\beta_1}|\alpha_1\rangle|\beta_1\rangle\right)\left(\sum_{\alpha_2,\beta_2} \overline{C}_{\alpha_2,\beta_2}\langle\alpha_2|\langle\beta_2|\right)\right]|\beta_3\rangle \tag{A.8}$$

$$= \sum_{\beta_3}\left[\left(\sum_{\alpha_1} C_{\alpha_1,\beta_3}|\alpha_1\rangle\right)\left(\sum_{\alpha_2} \overline{C}_{\alpha_2,\beta_3}\langle\alpha_2|\right)\right] \tag{A.9}$$

If we relabel $\beta_3 \to \beta_1$ and compute a matrix element:

$$\langle\alpha_1|\rho_{\mathrm{A}}|\alpha_2\rangle = \langle\alpha_1|\sum_{\beta_1}\left[\left(\sum_{\alpha_1} C_{\alpha_1,\beta_1}|\alpha_1\rangle\right)\left(\sum_{\alpha_2} \overline{C}_{\alpha_2,\beta_1}\langle\alpha_2|\right)\right]|\alpha_2\rangle \tag{A.10}$$

$$= \sum_{\beta_1} C_{\alpha_1,\beta_1}\overline{C}_{\alpha_2,\beta_1}, \tag{A.11}$$

you may notice that (A.11) is one of the expressions found in (A.5). Now we can continue the calculation of $\langle Swap_{\mathrm{A}}\rangle$.

$$\langle Swap_{\mathrm{A}}\rangle = \sum_{\alpha_1,\alpha_2}\left(\langle\alpha_1|\rho_{\mathrm{A}}|\alpha_2\rangle\langle\alpha_2|\rho_{\mathrm{A}}|\alpha_1\rangle\right) \tag{A.12}$$

$$= \sum_{\alpha_1}\Big(\langle\alpha_1|\rho_{\mathrm{A}}\underbrace{\sum_{\alpha_2}|\alpha_2\rangle\langle\alpha_2|}_{\mathbb{1}}\rho_{\mathrm{A}}|\alpha_1\rangle\Big) \tag{A.13}$$

$$= \sum_{\alpha_1}\langle\alpha_1|\rho_{\mathrm{A}}^2|\alpha_1\rangle \tag{A.14}$$

$$\boxed{\langle Swap_{\mathrm{A}}\rangle = \mathrm{Tr}(\rho_{\mathrm{A}}^2)} \tag{A.15}$$

Appendix B

Small-Scale Entropy Calculation

Here we find the von Neuman Entanglement Entropy (S^{vN}) of a state which is a linear combination (with equal parts) of all vertical and all horizontal valence bonds in a 2x4 site system. None of the bonds cross the boundary between subsystems A and B. The system is illustrated in the diagram below.

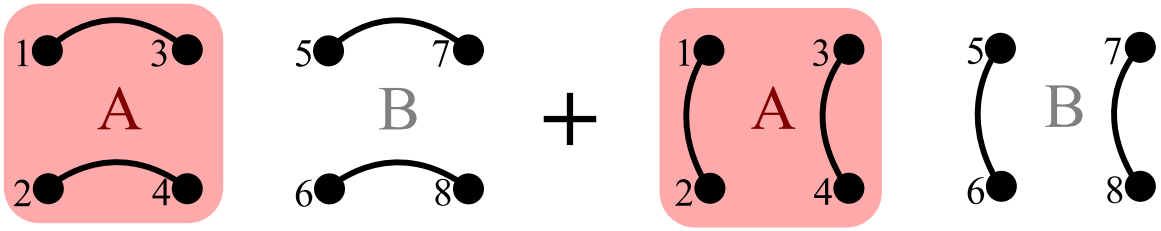

Figure B.1: An equal superposition of two eight-site states. Region A is the shaded region including sites $1-4$. Region B contains the remainder of the sites, $5-8$. For this state $S_{\mathrm{A}}^{\mathrm{VB}} = 0$ and $S_{\mathrm{A}}^{\mathrm{vN}} \approx 0.325$.

We start by writing out the wavefunction of the system, where C is the normalization constant.

$$\begin{aligned} |\psi\rangle \;=\; & C\left[(|\uparrow_1\downarrow_2\rangle - |\downarrow_1\uparrow_2\rangle)\otimes(|\uparrow_3\downarrow_4\rangle - |\downarrow_3\uparrow_4\rangle)\otimes(|\uparrow_5\downarrow_6\rangle - |\downarrow_5\uparrow_6\rangle)\otimes(|\uparrow_7\downarrow_8\rangle - |\downarrow_7\uparrow_8\rangle)\right] \\ & + C\left[(|\uparrow_1\downarrow_3\rangle - |\downarrow_1\uparrow_3\rangle)\otimes(|\uparrow_2\downarrow_4\rangle - |\downarrow_2\uparrow_4\rangle)\otimes(|\uparrow_5\downarrow_7\rangle - |\downarrow_5\uparrow_7\rangle)\otimes(|\uparrow_6\downarrow_8\rangle - |\downarrow_6\uparrow_8\rangle)\right] \end{aligned}$$

$$\begin{aligned} |\psi\rangle \;=\; & C\big[\,(|\uparrow_1\downarrow_2\uparrow_3\downarrow_4\rangle - |\uparrow_1\downarrow_2\downarrow_3\uparrow_4\rangle - |\downarrow_1\uparrow_2\uparrow_3\downarrow_4\rangle + |\downarrow_1\uparrow_2\downarrow_3\uparrow_4\rangle)\otimes \\ & \qquad (|\uparrow_5\downarrow_6\uparrow_7\downarrow_8\rangle - |\uparrow_5\downarrow_6\downarrow_7\uparrow_8\rangle - |\downarrow_5\uparrow_6\uparrow_7\downarrow_8\rangle + |\downarrow_5\uparrow_6\downarrow_7\uparrow_8\rangle)\,\big] \\ & + C\big[\,(|\uparrow_1\uparrow_2\downarrow_3\downarrow_4\rangle - |\uparrow_1\downarrow_2\downarrow_3\uparrow_4\rangle - |\downarrow_1\uparrow_2\uparrow_3\downarrow_4\rangle + |\downarrow_1\downarrow_2\uparrow_3\uparrow_4\rangle)\otimes \\ & \qquad (|\uparrow_5\uparrow_6\downarrow_7\downarrow_8\rangle - |\uparrow_5\downarrow_6\downarrow_7\uparrow_8\rangle - |\downarrow_5\uparrow_6\uparrow_7\downarrow_8\rangle + |\downarrow_5\downarrow_6\uparrow_7\uparrow_8\rangle)\,\big] \end{aligned}$$

$$
\begin{aligned}
|\psi\rangle &= C[\,|\uparrow_1\downarrow_2\uparrow_3\downarrow_4\rangle \otimes (|\uparrow_5\downarrow_6\uparrow_7\downarrow_8\rangle - |\uparrow_5\downarrow_6\downarrow_7\uparrow_8\rangle - |\downarrow_5\uparrow_6\uparrow_7\downarrow_8\rangle + |\downarrow_5\uparrow_6\downarrow_7\uparrow_8\rangle) \\
&\quad +|\uparrow_1\downarrow_2\downarrow_3\uparrow_4\rangle \otimes (-|\uparrow_5\downarrow_6\uparrow_7\downarrow_8\rangle + |\uparrow_5\downarrow_6\downarrow_7\uparrow_8\rangle + |\downarrow_5\uparrow_6\uparrow_7\downarrow_8\rangle - |\downarrow_5\uparrow_6\downarrow_7\uparrow_8\rangle) \\
&\quad +|\downarrow_1\uparrow_2\uparrow_3\downarrow_4\rangle \otimes (-|\uparrow_5\downarrow_6\uparrow_7\downarrow_8\rangle + |\uparrow_5\downarrow_6\downarrow_7\uparrow_8\rangle + |\downarrow_5\uparrow_6\uparrow_7\downarrow_8\rangle - |\downarrow_5\uparrow_6\downarrow_7\uparrow_8\rangle) \\
&\quad +|\downarrow_1\uparrow_2\downarrow_3\uparrow_4\rangle \otimes (|\uparrow_5\downarrow_6\uparrow_7\downarrow_8\rangle - |\uparrow_5\downarrow_6\downarrow_7\uparrow_8\rangle - |\downarrow_5\uparrow_6\uparrow_7\downarrow_8\rangle + |\downarrow_5\uparrow_6\downarrow_7\uparrow_8\rangle) \\
&\quad +|\uparrow_1\uparrow_2\downarrow_3\downarrow_4\rangle \otimes (|\uparrow_5\uparrow_6\downarrow_7\downarrow_8\rangle - |\uparrow_5\downarrow_6\downarrow_7\uparrow_8\rangle - |\downarrow_5\uparrow_6\uparrow_7\downarrow_8\rangle + |\downarrow_5\downarrow_6\uparrow_7\uparrow_8\rangle) \\
&\quad +|\uparrow_1\downarrow_2\downarrow_3\uparrow_4\rangle \otimes (-|\uparrow_5\uparrow_6\downarrow_7\downarrow_8\rangle + |\uparrow_5\downarrow_6\downarrow_7\uparrow_8\rangle + |\downarrow_5\uparrow_6\uparrow_7\downarrow_8\rangle - |\downarrow_5\downarrow_6\uparrow_7\uparrow_8\rangle) \\
&\quad +|\downarrow_1\uparrow_2\uparrow_3\downarrow_4\rangle \otimes (-|\uparrow_5\uparrow_6\downarrow_7\downarrow_8\rangle + |\uparrow_5\downarrow_6\downarrow_7\uparrow_8\rangle + |\downarrow_5\uparrow_6\uparrow_7\downarrow_8\rangle - |\downarrow_5\downarrow_6\uparrow_7\uparrow_8\rangle) \\
&\quad +|\downarrow_1\downarrow_2\uparrow_3\uparrow_4\rangle \otimes (|\uparrow_5\uparrow_6\downarrow_7\downarrow_8\rangle - |\uparrow_5\downarrow_6\downarrow_7\uparrow_8\rangle - |\downarrow_5\uparrow_6\uparrow_7\downarrow_8\rangle + |\downarrow_5\downarrow_6\uparrow_7\uparrow_8\rangle)\,] \\
&= C[\,|\uparrow_1\downarrow_2\uparrow_3\downarrow_4\rangle \otimes (|\uparrow_5\downarrow_6\uparrow_7\downarrow_8\rangle - |\uparrow_5\downarrow_6\downarrow_7\uparrow_8\rangle - |\downarrow_5\uparrow_6\uparrow_7\downarrow_8\rangle + |\downarrow_5\uparrow_6\downarrow_7\uparrow_8\rangle) \\
&\quad +|\uparrow_1\downarrow_2\downarrow_3\uparrow_4\rangle \otimes (-|\uparrow_5\downarrow_6\uparrow_7\downarrow_8\rangle + 2|\uparrow_5\downarrow_6\downarrow_7\uparrow_8\rangle + 2|\downarrow_5\uparrow_6\uparrow_7\downarrow_8\rangle - |\downarrow_5\uparrow_6\downarrow_7\uparrow_8\rangle \\
&\qquad\qquad -|\uparrow_5\uparrow_6\downarrow_7\downarrow_8\rangle - |\downarrow_5\downarrow_6\uparrow_7\uparrow_8\rangle) \\
&\quad +|\downarrow_1\uparrow_2\uparrow_3\downarrow_4\rangle \otimes (-|\uparrow_5\downarrow_6\uparrow_7\downarrow_8\rangle + 2|\uparrow_5\downarrow_6\downarrow_7\uparrow_8\rangle + 2|\downarrow_5\uparrow_6\uparrow_7\downarrow_8\rangle - |\downarrow_5\uparrow_6\downarrow_7\uparrow_8\rangle \\
&\qquad\qquad -|\uparrow_5\uparrow_6\downarrow_7\downarrow_8\rangle - |\downarrow_5\downarrow_6\uparrow_7\uparrow_8\rangle) \\
&\quad +|\downarrow_1\uparrow_2\downarrow_3\uparrow_4\rangle \otimes (|\uparrow_5\downarrow_6\uparrow_7\downarrow_8\rangle - |\uparrow_5\downarrow_6\downarrow_7\uparrow_8\rangle - |\downarrow_5\uparrow_6\uparrow_7\downarrow_8\rangle + |\downarrow_5\uparrow_6\downarrow_7\uparrow_8\rangle) \\
&\quad +|\uparrow_1\uparrow_2\downarrow_3\downarrow_4\rangle \otimes (|\uparrow_5\uparrow_6\downarrow_7\downarrow_8\rangle - |\uparrow_5\downarrow_6\downarrow_7\uparrow_8\rangle - |\downarrow_5\uparrow_6\uparrow_7\downarrow_8\rangle + |\downarrow_5\downarrow_6\uparrow_7\uparrow_8\rangle) \\
&\quad +|\downarrow_1\downarrow_2\uparrow_3\uparrow_4\rangle \otimes (|\uparrow_5\uparrow_6\downarrow_7\downarrow_8\rangle - |\uparrow_5\downarrow_6\downarrow_7\uparrow_8\rangle - |\downarrow_5\uparrow_6\uparrow_7\downarrow_8\rangle + |\downarrow_5\downarrow_6\uparrow_7\uparrow_8\rangle)\,]
\end{aligned}
$$

Now we can normalize the state.

$$
\begin{aligned}
\langle\psi|\psi\rangle &= C^2 = 4\times(1+1+1+1) + 2\times(1+4+4+1+1+1) \\
&= 40
\end{aligned}
$$

For simplicity we relabel the states.

$$
\begin{aligned}
|a\rangle &= |\uparrow_5\downarrow_6\uparrow_7\downarrow_8\rangle & |c\rangle &= |\downarrow_5\uparrow_6\uparrow_7\downarrow_8\rangle & |e\rangle &= |\uparrow_5\uparrow_6\downarrow_7\downarrow_8\rangle \\
|b\rangle &= |\uparrow_5\downarrow_6\downarrow_7\uparrow_8\rangle & |d\rangle &= |\downarrow_5\uparrow_6\downarrow_7\uparrow_8\rangle & |f\rangle &= |\downarrow_5\downarrow_6\uparrow_7\uparrow_8\rangle
\end{aligned}
$$

Now a few steps are skipped as we trace out region A of the system to get the reduced density matrix of region B.

$$
\begin{aligned}
\rho_{\rm B} &= {\rm Tr}_A|\psi\rangle\langle\psi| \\
&= \frac{1}{40}\Bigg[\, 2\times\Big(|a\rangle - |b\rangle - |c\rangle + |d\rangle\Big)\Big(\langle a| - \langle b| - \langle c| + \langle d|\Big) \\
&\quad + \;\; 2\times\Big(|e\rangle - |b\rangle - |c\rangle + |f\rangle\Big)\Big(\langle e| - \langle b| - \langle c| + \langle f|\Big) \\
&\quad + \;\; 2\times\Big(|a\rangle - 2|b\rangle - 2|c\rangle + |d\rangle + |e\rangle + |f\rangle\Big)\Big(\langle a| - 2\langle b| - 2\langle c| + \langle d| + \langle e| + \langle f|\Big)\,\Bigg]
\end{aligned}
$$

$$
\begin{aligned}
\rho_{\mathrm{B}} \;=\; \frac{1}{20}\Big[& \;\; |a\rangle\langle a| - |a\rangle\langle b| - |a\rangle\langle c| + |a\rangle\langle d| \;\; - \;\; |b\rangle\langle a| + |b\rangle\langle b| + |b\rangle\langle c| - |b\rangle\langle d| \\
& - |c\rangle\langle a| + |c\rangle\langle b| + |c\rangle\langle c| - |c\rangle\langle d| \;\; + \;\; |d\rangle\langle a| - |d\rangle\langle b| - |d\rangle\langle c| + |d\rangle\langle d| \\
& + |e\rangle\langle e| - |e\rangle\langle b| - |e\rangle\langle c| + |e\rangle\langle f| \;\; - \;\; |b\rangle\langle e| + |b\rangle\langle b| + |b\rangle\langle c| - |b\rangle\langle f| \\
& - |c\rangle\langle e| + |c\rangle\langle b| + |c\rangle\langle c| - |c\rangle\langle f| \;\; + \;\; |e\rangle\langle e| - |e\rangle\langle b| - |e\rangle\langle c| + |e\rangle\langle f| \\
& + |a\rangle\langle a| -2\,|a\rangle\langle b| -2\,|a\rangle\langle c| + |a\rangle\langle d| + |a\rangle\langle e| + |a\rangle\langle f| \\
& -2\,|b\rangle\langle a| +4\,|b\rangle\langle b| +4\,|b\rangle\langle c| -2\,|b\rangle\langle d| -2\,|b\rangle\langle e| -2\,|b\rangle\langle f| \\
& -2\,|c\rangle\langle a| +4\,|c\rangle\langle b| +4\,|c\rangle\langle c| -2\,|c\rangle\langle d| -2\,|c\rangle\langle e| -2\,|c\rangle\langle f| \\
& + |d\rangle\langle a| -2\,|d\rangle\langle b| -2\,|d\rangle\langle c| + |d\rangle\langle d| + |d\rangle\langle e| + |d\rangle\langle f| \\
& + |e\rangle\langle a| -2\,|e\rangle\langle b| -2\,|e\rangle\langle c| + |e\rangle\langle d| + |e\rangle\langle e| + |e\rangle\langle f| \\
& + |f\rangle\langle a| -2\,|f\rangle\langle b| -2\,|f\rangle\langle c| + |f\rangle\langle d| + |f\rangle\langle e| + |f\rangle\langle f| \;\; \Big]
\end{aligned}
$$

$$
\begin{aligned}
= \; \frac{1}{20}\Big[& \;\; 2\,|a\rangle\langle a| -3\,|a\rangle\langle b| -3\,|a\rangle\langle c| +2\,|a\rangle\langle d| \;\; + |a\rangle\langle e| \;\; + |a\rangle\langle f| \\
& -3\,|b\rangle\langle a| +6\,|b\rangle\langle b| \;+6\,|b\rangle\langle c| -3\,|b\rangle\langle d| \;-3\,|b\rangle\langle e| -3\,|b\rangle\langle f| \\
& -3\,|c\rangle\langle a| +6\,|c\rangle\langle b| \;+6\,|c\rangle\langle c| -3\,|c\rangle\langle d| \;-3\,|c\rangle\langle e| -3\,|c\rangle\langle f| \\
& +2\,|d\rangle\langle a| -3\,|d\rangle\langle b| -3\,|d\rangle\langle c| +2\,|d\rangle\langle d| \;\; + |d\rangle\langle e| \;\; + |d\rangle\langle f| \\
& + \;\; |e\rangle\langle a| \;-3\,|e\rangle\langle b| -3\,|e\rangle\langle c| \;\; + |e\rangle\langle d| +2\,|e\rangle\langle e| \;+2\,|e\rangle\langle f| \\
& + \;\; |f\rangle\langle a| -3\,|f\rangle\langle b| -3\,|f\rangle\langle c| \;+ |f\rangle\langle d| +2\,|f\rangle\langle e| +2\,|f\rangle\langle f| \;\; \Big]
\end{aligned}
$$

$$
= \; \frac{1}{20}\begin{bmatrix}
2 & -3 & -3 & 2 & 1 & 1 \\
-3 & 6 & 6 & -3 & -3 & -3 \\
-3 & 6 & 6 & -3 & -3 & -3 \\
2 & -3 & -3 & 2 & 1 & 1 \\
1 & -3 & -3 & 1 & 2 & 2 \\
1 & -3 & -3 & 1 & 2 & 2
\end{bmatrix}
$$

The matrix $\rho_{\rm B}$ was diagonalized using MATLAB.

$$\rho_{\rm B}^{\rm diag} = \frac{1}{10}\begin{bmatrix} 9 & 0 & 0 & 0 & 0 & 0 \\ 0 & 1 & 0 & 0 & 0 & 0 \\ 0 & 0 & 0 & 0 & 0 & 0 \\ 0 & 0 & 0 & 0 & 0 & 0 \\ 0 & 0 & 0 & 0 & 0 & 0 \\ 0 & 0 & 0 & 0 & 0 & 0 \end{bmatrix}$$

We can finally compute the entanglement entropy.

$$S_{\rm B}^{\rm vN} = -{\rm Tr}\left(\rho_{\rm B}{\rm ln}\rho_{\rm B}\right) = -{\rm Tr}(\rho_{\rm B}^{\rm diag}{\rm ln}\rho_{\rm B}^{\rm diag})$$

$$= -{\rm Tr}\left(\begin{bmatrix} 0.9 & 0 & 0 & 0 & 0 & 0 \\ 0 & 0.1 & 0 & 0 & 0 & 0 \\ 0 & 0 & 0 & 0 & 0 & 0 \\ 0 & 0 & 0 & 0 & 0 & 0 \\ 0 & 0 & 0 & 0 & 0 & 0 \\ 0 & 0 & 0 & 0 & 0 & 0 \end{bmatrix} {\rm ln}\left(\begin{bmatrix} 0.9 & 0 & 0 & 0 & 0 & 0 \\ 0 & 0.1 & 0 & 0 & 0 & 0 \\ 0 & 0 & 0 & 0 & 0 & 0 \\ 0 & 0 & 0 & 0 & 0 & 0 \\ 0 & 0 & 0 & 0 & 0 & 0 \\ 0 & 0 & 0 & 0 & 0 & 0 \end{bmatrix}\right)\right)$$

$$= -0.9{\rm ln}(0.9) - 0.1{\rm ln}(0.1) \approx 0.325 \neq S_{\rm B}^{\rm VB} = 0$$

References

[1] Scott Hill and William K. Wootters. Entanglement of a pair of quantum bits. *Phys. Rev. Lett.*, 78(26):5022–5025, Jun 1987. 2

[2] M. B. Plenio. Logarithmic negativity: A full entanglement monotone that is not convex. *Phys. Rev. Lett.*, 95(9):090503, Aug 2005. 2

[3] Matthias Christandl and Andreas Winter. "squashed entanglement": An additive entanglement measure. *Journal of Mathematical Physics*, 45(3):829–840, 2004. 2

[4] Charles H. Bennett, Herbert J. Bernstein, Sandu Popescu, and Benjamin Schumacher. Concentrating partial entanglement by local operations. *Phys. Rev. A*, 53(4):2046–2052, Apr 1996. 2

[5] Martin B. Plenio and S. Virmani. An introduction to entanglement measures. *ArXiv Quantum Physics e-prints*, page 25, April 2005. 2

[6] Christian Beck and Friedrich Schogl. *Thermodynamics of Chaotic Systems*. Cambridge University Press, 1995. 3

[7] Luigi Amico, Rosario Fazio, Andreas Osterloh, and Vlatko Vedral. Entanglement in many-body systems. *Reviews of Modern Physics*, 80(2):517–576, May 2008. 3

[8] Andreas M Läuchli, Emil J Bergholtz, and Masudul Haque. Entanglement scaling of fractional quantum hall states through geometric deformations. *New Journal of Physics*, 12(7):075004, 2010. 3

[9] Mark Srednicki. Entropy and area. *Phys. Rev. Lett.*, 71(5):666–669, Aug 1993. 4

[10] J. Eisert, M. Cramer, and M. B. Plenio. Colloquium: Area laws for the entanglement entropy. *Rev. Mod. Phys.*, 82(1):277–306, Feb 2010. 4, 27

[11] Steven T. Flammia, Alioscia Hamma, Taylor Bieber Hughes, and Xiao-Gang Wen. Topological entanglement rényi entropy and reduced density matrix structure. *Phys. Rev. Lett.*, 103(26):261601, Dec 2009. 4, 5, 39

[12] Pasquale Calabrese and John Cardy. Entanglement entropy and quantum field theory. *J. Stat. Mech.: Theor. Exp.*, 2004(06):P06002, 2004. 4, 29

[13] Nicolas Laflorencie, Erik S. Sørensen, Ming-Shyang Chang, and Ian Affleck. Boundary effects in the critical scaling of entanglement entropy in 1d systems. *Phys. Rev. Lett.*, 96(10):100603, Mar 2006. 4, 27, 29, 31

[14] Huan-Qiang Zhou, Thomas Barthel, John Fjærestad, and Ulrich Schollwöck. Entanglement and boundary critical phenomena. *Physical Review A*, 74(5):1–4, November 2006. 4, 29

[15] Ian Affleck and Andreas W. W. Ludwig. Universal noninteger ‘‘ground-state degeneracy’’ in critical quantum systems. *Phys. Rev. Lett.*, 67(2):161–164, Jul 1991. 4

[16] Alexei Kitaev and John Preskill. Topological entanglement entropy. *Phys. Rev. Lett.*, 96(11):110404, Mar 2006. 5

[17] Michael Levin and Xiao-Gang Wen. Detecting topological order in a ground state wave function. *Phys. Rev. Lett.*, 96(11):110405, Mar 2006. 5

[18] H. Casini and M. Huerta. Universal terms for the entanglement entropy in 2+1 dimensions. *Nuclear Physics B*, 764(3):183 – 201, 2007. 5

[19] Shinsei Ryu and Tadashi Takayanagi. Holographic derivation of entanglement entropy from the anti–de sitter space/conformal field theory correspondence. *Phys. Rev. Lett.*, 96(18):181602, May 2006. 5

[20] Max A. Metlitski, Carlos A. Fuertes, and Subir Sachdev. Entanglement entropy in the $o(n)$ model. *Phys. Rev. B*, 80(11):115122, Sep 2009. 5

[21] Anders W. Sandvik. Ground state projection of quantum spin systems in the valence-bond basis. *Phys. Rev. Lett.*, 95(20):207203, Nov 2005. 6, 20, 22, 27

[22] A. W. Sandvik and K. S. D. Beach. Monte Carlo Simulations of Quantum Spin Systems in the Valence Bond Basis. *ArXiv Quantum Physics e-prints*, page 15, April 2007. 6, 27

[23] Olav F. Syljuåsen and Anders W. Sandvik. Quantum monte carlo with directed loops. *Phys. Rev. E*, 66(4):046701, Oct 2002. 6

[24] H. G. Evertz. The loop algorithm. *Advances in Physics*, 52(1):1 – 66, 2003. 6

[25] P. W. Anderson. Resonating valence bonds: A new kind of insulator? *Materials Research Bulletin*, 8(2):153 – 160, 1973. 6

[26] P. Fazekas and P. W. Anderson. On the ground state properties of the anisotropic triangular antiferromagnet. *Philosophical Magazine*, 30(2):423 – 440, 1974. 6

[27] J. Slater. Molecular Energy Levels and Valence Bonds. *Physical Review*, 38(6):1109–1144, September 1931. 8

[28] Linus Pauling. The Calculation of Matrix Elements for Lewis Electronic Structures of Molecules. *The Journal of Chemical Physics*, 1(4):280, 1933. 8

[29] K. S. D. Beach and A. W. Sandvik. Some formal results for the valence bond basis. *Nuclear Physics B*, 750(3):142–178, August 2006. 11, 13, 24

[30] C. Lanczos. An iteration method for the solution of the eigenvalue problem of linear differential and integral operators. *Journal of research of the National Bureau of Standards*, 45(4):255–282, 1950. 17

[31] W. M. C. Foulkes, L. Mitas, R. J. Needs, and G. Rajagopal. Quantum monte carlo simulations of solids. *Rev. Mod. Phys.*, 73(1):33–83, Jan 2001. 17

[32] David Ceperley and Berni Alder. Quantum monte carlo. *Science*, 231(4738):pp. 555–560, 1986. 17

[33] A. W. Sandvik and H. G. Evertz. Loop updates for valence-bond projector quantum Monte Carlo simulations. *arXiv:0807.0682*, page 4, July 2008. 24

[34] Anders W. Sandvik and Hans Gerd Evertz. Loop updates for variational and projector quantum monte carlo simulations in the valence-bond basis. *Phys. Rev. B*, 82(2):024407, Jul 2010. 24, 31

[35] Fabien Alet, Sylvain Capponi, Nicolas Laflorencie, and Matthieu Mambrini. Valence bond entanglement entropy. *Phys. Rev. Lett.*, 99(11):117204, Sep 2007. 27, 36, 38, 47

[36] Ravindra W. Chhajlany, Piotr Tomczak, and Antoni Wójcik. Topological estimator of block entanglement for heisenberg antiferromagnets. *Phys. Rev. Lett.*, 99(16):167204, Oct 2007. 27, 31, 36, 38, 47

[37] Niel de Beaudrap, Tobias J Osborne, and Jens . Ground states of unfrustrated spin Hamiltonians satisfy an area law. *New Journal of Physics*, 12(9):095007, September 2010. 27

[38] Ann B. Kallin, Iván González, Matthew B. Hastings, and Roger G. Melko. Valence bond and von neumann entanglement entropy in heisenberg ladders. *Phys. Rev. Lett.*, 103(11):117203, Sep 2009. 27, 47, 51

[39] U. Schollwöck. The density-matrix renormalization group. *Rev. Mod. Phys.*, 77(1):259–315, Apr 2005. 27

[40] Steven R. White. Density matrix formulation for quantum renormalization groups. *Phys. Rev. Lett.*, 69(19):2863–2866, Nov 1992. 27

[41] J. I. Latorre, E. Rico, and G. Vidal. Ground state entanglement in quantum spin chains. *ArXiv Quantum Physics e-prints*, April 2003. 31

[42] J. L. Jacobsen and H. Saleur. Exact valence bond entanglement entropy and probability distribution in the xxx spin chain and the potts model. *Phys. Rev. Lett.*, 100(8):087205, Feb 2008. 31, 38

[43] S. R. White, R. M. Noack, and D. J. Scalapino. Resonating valence bond theory of coupled heisenberg chains. *Phys. Rev. Lett.*, 73(6):886–889, 1994. 31

[44] Matthew B. Hastings, Iván González, Ann B. Kallin, and Roger G. Melko. Measuring renyi entanglement entropy in quantum monte carlo simulations. *Phys. Rev. Lett.*, 104(15):157201, Apr 2010. 39

[45] Roger G. Melko, Ann B. Kallin, and Matthew B. Hastings. Finite-size scaling of mutual information in monte carlo simulations: Application to the spin- $\frac{1}{2}$ xxz model. *Phys. Rev. B*, 82(10):100409, Sep 2010. 40, 53

[46] Bernd A. Berg and Thomas Neuhaus. Multicanonical ensemble: A new approach to simulate first-order phase transitions. *Phys. Rev. Lett.*, 68(1):9, Jan 1992. 53

[47] Bernd A. Berg and Thomas Neuhaus. Multicanonical algorithms for first order phase transitions. *Physics Letters B*, 267(2):249 – 253, 1991. 53

[48] Michael M. Wolf, Frank Verstraete, Matthew B. Hastings, and J. Ignacio Cirac. Area laws in quantum systems: Mutual information and correlations. *Phys. Rev. Lett.*, 100(7):070502, Feb 2008.

[49] F. Verstraete and J. I. Cirac. Renormalization algorithms for quantum-many body systems in two and higher dimensions. *arXiv:cond-mat/0407066*, 2004.

[50] F. Verstraete, M. M. Wolf, D. Perez-Garcia, and J. I. Cirac. Criticality, the area law, and the computational power of projected entangled pair states. *Phys. Rev. Lett.*, 96(22):220601, Jun 2006.

[51] Stellan Östlund and Stefan Rommer. Thermodynamic limit of density matrix renormalization. *Phys. Rev. Lett.*, 75(19):3537–3540, Nov 1995.

[52] G. Evenbly and G. Vidal. Algorithms for entanglement renormalization. *Phys. Rev. B*, 79(14):144108, Apr 2009.

[53] Hui Li and F. D. M. Haldane. Entanglement spectrum as a generalization of entanglement entropy: Identification of topological order in non-abelian fractional quantum hall effect states. *Phys. Rev. Lett.*, 101(1):010504, Jul 2008.

[54] Eduardo Fradkin and Joel E. Moore. Entanglement entropy of 2d conformal quantum critical points: Hearing the shape of a quantum drum. *Phys. Rev. Lett.*, 97(5):050404, Aug 2006.

[55] Curtis Callan and Frank Wilczek. On geometric entropy. *Physics Letters B*, 333(1-2):55 – 61, 1994.